CHEMICAL REVIEWS

Review

pubs.acs.org/CR

Synthesis of Metal Oxide Nanostructures by Direct Sol–Gel Chemistry in Supercritical Fluids

Ruohong Sui[†] and Paul Charpentier[‡,*]

[†]Alberta Sulphur Research Ltd., University of Calgary, 6-3535 Research Road, N.W., Calgary, Alberta, Canada T2L 2K8

[‡]Department of Chemical and Biochemical Engineering, University of Western Ontario, London, Ontario, Canada N6A 5B9

CONTENTS

1. INTRODUCTION

Nanoscale metal oxides are of tremendous current interest to scientists and engineers because of the potential of their emerging applications spanning from catalysts, sensors, and microelectronic devices to energy conversion devices including solar and fuel cells.[1−7] One critical component of catalysts (active phase, promoter, or support) is the metal oxide that plays an important role in the chemical, petrochemical, and environmental industries. Examples of common commercial metal oxides include Al_2O_3, SiO_2, and TiO_2, which have unique chemical, physical and catalytic properties. In addition, many metal oxides (e.g., K_2O, MgO, BaO, Al_2O_3, PbO, TiO_2, ZrO_2, MoO_2, CuO, and V_2O_5) are either active phases or catalyst promoters in a wide range of reactions.[8,9] TiO_2 and ZnO films composed of nanospheres, nanowires or nanotube arrays, can function as semiconductors for photon-generated electron carriers, and have been used in dye-sensitized solar cells (DSSCs) to promote electron transport.[3,10,11] Moreover, metal oxide nanowires and atomic layer deposition techniques have the potential to be used for the miniaturization of microelectronic chips.[12−14] The inherent characteristics of the metal oxide, in the form of nanoparticles, for example, large surface-to-volume ratio and a Debye length comparable to their dimensions, enhances their usefulness in these emerging applications.[13,15]

To produce this next generation of metal oxide nanomaterials, a variety of synthetic approaches have been investigated: precipitation,[16] decomposition,[17] chemical vapor deposition (CVD),[18] template-assisted synthesis,[19] electrochemical,[20] electronspinning,[21] hydrothermal,[22] reverse micelle,[23] and sol–gel techniques.[24] Only a few of these methods are under consideration for industrial-scale production due to the relatively high capital investment, operational costs and safety issues. To produce important industrial catalysts such as Degussa P-25 (TiO_2 nanoparticles) which is recognized as a benchmark photocatalyst, $TiCl_4$ is pyrolyzed at high-temperatures.[25] However, one disadvantage is that this process is known to have a relatively low yield. Another example is the calcination of aluminum hydroxide precipitate which is widely used industrially for producing alumina hydrates and alumina with different crystalline phases, for example, β, γ, η, χ, κ, δ, and θ-alumina and ultimately α-alumina.[8] However, in this case when the precipitate method is used it is difficult to control the morphology of the resulting materials.

Originally used for synthesizing high-quality SiO_2, sol–gel processes have emerged as a standard production method for metal/silicon oxide nanomaterials with various morphologies. The advantages of sol–gel methods include: their high yield, low operation temperatures and low production costs.[8,26−28] The sol–gel process is generally considered as "soft chemistry" in contrast to more classical industrial techniques for glass and ceramic manufacturing which require very high temperatures.[29] This review aims at covering direct sol–gel reactions in supercritical fluids (SCFs) for the synthesis of metal/silicon oxides with different geometries on a nanometer scale. The emphasis is on the physics, chemistry, and engineering aspects of the polycondensation of metal oxide precursors in SCFs while highlighting the mechanisms of both the chemical

Received: February 6, 2011
Published: March 7, 2012

   dx.doi.org/10.1021/cr2000465 | Chem. Rev. 2012, 112, 3057–3082

reactions and nanostructure formation. These examples will hopefully not only illustrate the feasibility and importance of SCFs for the future of advanced metal oxide production within the context of a sustainable future, but also encourage further exploration in this important emerging field.

2. SUPERCRITICAL FLUIDS AND DIRECT SOL–GEL CHEMISTRY

2.1. Supercritical Fluids and Supercritical Drying

2.1.1. Supercritical Fluid. A supercritical fluid (SCF) is defined as a single fluid phase which occurs when the temperature and pressure of a compound or mixture is above its critical temperature and pressure (T_c and P_c).[30] In this review, we refer to a SCF as a fluid not only in the region above its critical point (the green area in Scheme 1), but also close to the critical point where the SCF properties apply.[31]

Scheme 1. Schematic Drawing of Supercritical Fluid Region in the Phase Diagram of a Single Component

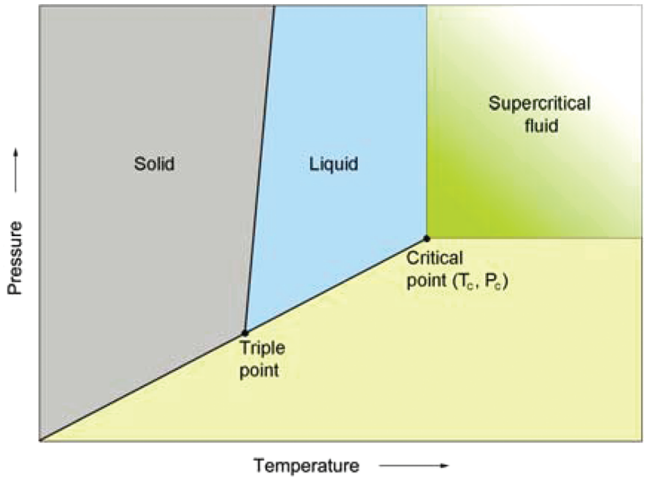

A SCF exhibits many superior physical properties compared to the liquid and gas phases for the synthesis of solid nanostructures using chemical reactions.[32] First, the solubility of a solute in a SCF is a function of the fluid density, which is tunable by manipulating the pressure and temperature. Second, SCFs exhibit low gas-like viscosities that enhance both mass and heat transfer which in turn accelerates the reaction kinetics (Table 1). Hence, both the reaction equilibrium (which is related to solubility) and the reaction rates can be tuned by adjusting the temperature and/or pressure.[33,34] This will be discussed in more depth later in this review. Construction of nanostructures through the solid–liquid interface, for example, decoration of secondary metal/oxide nanoparticles on a catalyst support, is often limited by the poor contact of the liquid with the solid surface. The surface tension of a solid-SCF interface is significantly smaller than that from a solid–liquid interface. Therefore this provides better "wetting" of the surface which in turn allows penetration of the reactants into the porous structure thus facilitating nanostructure formation.[35] Many reactions, such as the hydrolysis and condensation of metal salts for making metal oxides, are very slow in conventional solvents. When SCFs, such as supercritical alcohols or acetone, are used, the reaction temperature can reach a much higher level than in a conventional solvent under ambient pressure (Table 2). Such elevated temperatures can facilitate the formation of metal oxide materials within a very short time; thus making continuous reactor design feasible. In addition, SCFs have zero surface tension because there is only one phase (Figure 1), and this makes it possible to maintain the nanoscale architecture upon removal of the solvent during drying.[35] Finally, separation of the SCF and products at the end of the reaction can be conveniently achieved by simple depressurization.[36]

Table 1. Selected Viscosities and Densities of CO_2 in Vapor, Liquid, and Supercritical Phases[37]

temp (K)	pressure (MPa)	phase	viscosity (10^{-6} Pa·S)	density (kg/m^3)
313	6.9	vapor	19.1	192.5
303	20.7	liquid	90.5	896.1
323	13.8	supercritical	52.5	667.0
333	13.8	supercritical	41.3	552.6
333	34.5	supercritical	82.8	860.3

Table 2. Critical Data for Fluids Used in SCF Sol–Gel Processes

fluid	T_c (K)	P_c (MPa)	ρ_c (kg/m^3)
CO_2	304.2	7.375	468
H_2O	647.3	22.06	322
MeOH	513.7	8.092	272
EtOH	516.3	6.137	276
^{i}PrOH	508.5	4.762	273
acetone	508.2	4.66	273
NH_3	405.6	11.35	235

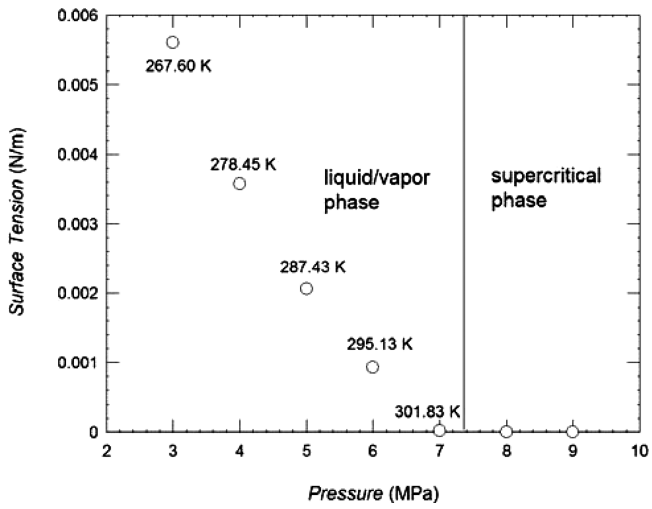

Figure 1. Surface tension of saturation liquid CO_2 vs pressure. The data points are labeled with the corresponding saturation temperatures at specific pressures. In the two phase region, the surface tension of the condensed phase decreases when the state is close to the supercritical condition. In the supercritical region, there is only one phase and the surface tension is zero.

In the rapidly developing field of SCF technology, one goal is to produce materials that have superior properties compared to those synthesized using conventional solvents at ambient pressure. Such properties include higher specific surface areas, and high porosities as well as well-defined nanostructures that remain intact after the supercritical drying process. Several

dx.doi.org/10.1021/cr2000465 | Chem. Rev. 2012, 112, 3057–3082

comprehensive reviews for SCF applications have appeared: in polymerization by DeSimone et al,[38] for the formation of metal−organic complexes by Poliakoff et al,[39] for the preparation of metal and semiconductor nanocrystals by Johnston and Korgel et al,[40] as well as for the synthesis of inorganic materials,[41] composite nanoparticles,[42] nanoparticle processing.[43,44] Others cover SCFs as a media for a range of chemical reactions.[30,32,45,46]

2.1.2. Supercritical Drying. Drying is often a necessary step in solid product synthesis. In the ambient pressure drying process, some shrinkage of the solid is inevitable and this leads to microstructure collapse resulting in low specific surface areas.[47] This solid microstructure collapse is induced by capillary forces which in turn result from the existence of a liquid−gas interface inside the pores among the solid-phase network. This aspect has been reviewed by Scherer[48] and Bisson et al.[49] Interestingly, using TEM, the meniscus between the gas−liquid phases has been observed in closed carbon nanotubes. This provides evidence of the capillary force exerted on the nanoscale channels (Figure 2). In a simple model of a

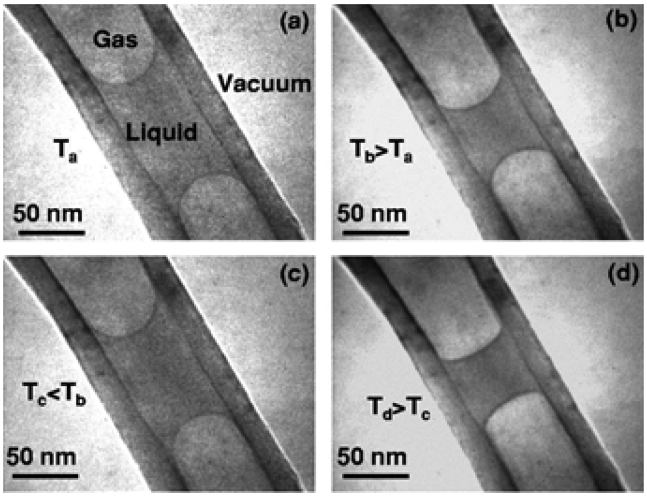

Figure 2. TEM micrograph sequence of a typical carbon nanotube section showing the reversible volume contraction/expansion of liquid entrapment upon heating/cooling achieved by manipulating the illuminating electron beam. (a) Initial shape of liquid at temperature T_a, (b) inclusion gets thinner upon heating at $T_b > T_a$, (c) liquid returns to its initial size upon cooling at $T_c < T_b$, (d) heating is repeated ($T_d > T_c$), resulting a renewed contraction of the liquid volume. Reproduced with permission from ref 50. Copyright 2001 EBSCO Publishing.

cylindrical pore, the capillary tension, P_{cap}, exerted by a meniscus of liquid is represented by

$$P_{cap} = -\frac{2\gamma_{LV}}{r} \quad (1)$$

Here, γ_{LV} is the liquid−vapor interfacial tension, and r is the radius of curvature of the meniscus. The capillary tension P_{cap} causes the pores to shrink and the solid network to contract into the liquid phase until tension by the liquid cannot overcome the stiffening of the solid network. This type of problem can be solved by supercritical drying.

Since the discovery by Kistler of using supercritical drying for making SiO_2 aerogels, and metal oxide materials,[51] it has become a common protocol for maintaining the solid phase microstructure. Supercritical drying used as a conventional unit operation has already been reviewed by others,[52−56] but it is still worth briefly examining here because of its role as an integral component of the direct sol−gel synthesis approach.

Because of the fact that in a SCF, the fluid is a single phase, SCF drying circumvents the liquid−gas interface during vaporization, hence preventing collapse of the solid network from capillary forces during the drying process (Figure 3). The

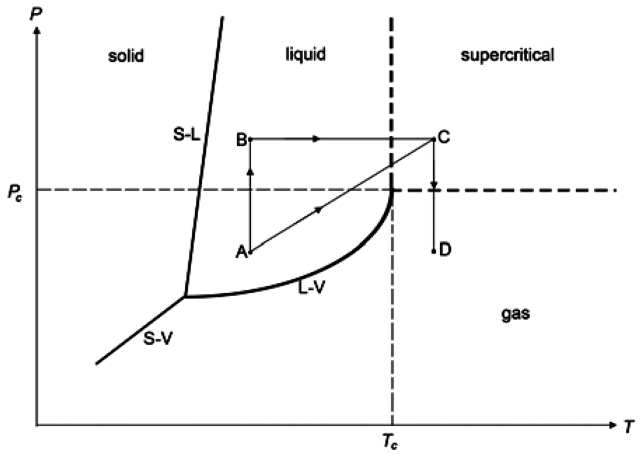

Figure 3. Schematic representation of supercritical drying: the solvent is pressurized and heated beyond the critical point (P_c, T_c) via one of two pathways either path ABC or path AC. This is followed by depressurization (path CD). In this way the interface of gas and liquid is circumvented. S−L, L−V, and S−V denote solid−liquid, liquid−vapor, and solid−vapor equilibrium curves, respectively.

supercritical drying process consists of three important steps: (1) pressurization by SCF that is combined with heating. This achieves one fluid phase by diffusion of the liquid from the pores into the SCF phase (A → C or A → B → C in Figure 3). (2) Continuous flushing with fresh SCF is used to remove organic solvents or H_2O, and (3) depressurization is used to remove the fluid phase (C → D in Figure 3). It should be noted that the heating in A → C or B → C and depressurization in C → D must be slow enough to avoid shear stress and consequent cracks in the nanostructure.[57,58]

To design a drying process, two parameters need to be considered: the solubility[59] and the diffusivity of the solvents (including organic species and water) in the SCF. The solubility of materials for direct sol−gel processing is described in detail later in this review. In terms of diffusivity, there are a number of models available for estimating transport properties in SCFs.[60] For example, the vapor−liquid diffusion during the $scCO_2$ drying process has been modeled using Fick's law in the one-dimensional form. The results show that the Fickian diffusivity is a strong function of the temperature whereas the pressure has a lower impact. This suggests that a higher temperature is favorable for mass transfer in the drying process while pressure has little effect.[61] It should be noted that a higher pressure has, however, an effect on the solubility of the organic species and H_2O, and this also needs to be considered when the amount of these species is significant.

2.2. Direct Sol−Gel Reactions in Supercritical Fluids

As the heading implies, sol−gel processes involve both sol and gel components. The sol is a colloidal suspension of nanometer-sized solid particles in a liquid phase. When these particles attract one another, under the correct conditions, they bond together forming a three-dimensional network called a

dx.doi.org/10.1021/cr2000465 | Chem. Rev. 2012, 112, 3057−3082

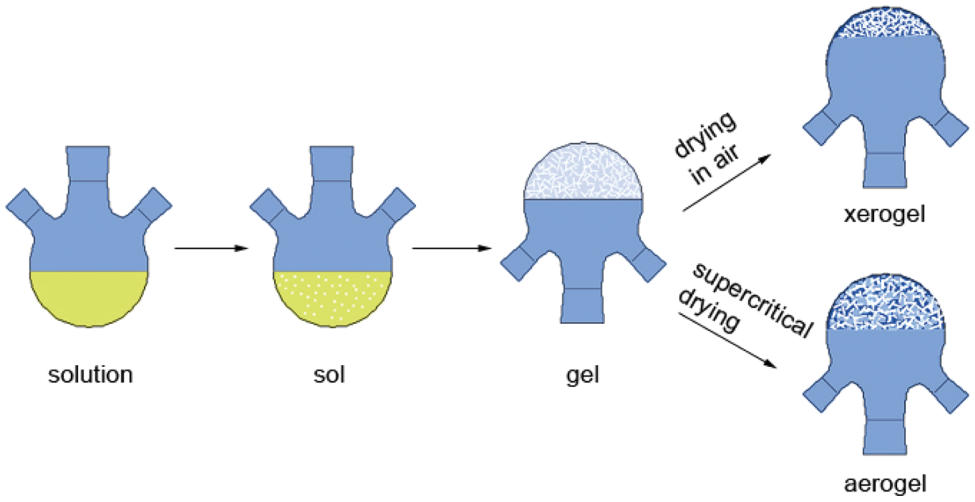

Figure 4. Schematic illustration of the formation of a sol in a liquid phase, a gel that has infinite viscosity, a xerogel that shrinks, and an aerogel without shrinkage.

gel. This contains a continuous solid skeleton enclosing a continuous liquid phase.[56] If the smallest dimension of the gel is greater than a few millimeters, the material is called a monolith. If the gels have dimensions spanning from a few nanometers to a few millimeters, they are called a particulate gel. Drying the gel by evaporation under ambient pressure gives rise to capillary pressure that causes shrinkage of the network, and the resulting materials are called xerogels. These are relatively dense with low surface areas. In contrast, drying the gel under supercritical conditions eliminates the interface between the liquid and vapor phases, and the resulting materials are called aerogels (Figure 4).

The first gel derived from a metal alkoxide was synthesized by Ebelmen as early as 1846,[62] whereas the first aerogels were prepared by Kistler in 1932.[51] A typical aerogel is comprised of both meso- (2−50 nm in diameter) and micropores (<2 nm in diameter). It exhibits a large surface area of hundreds of square meters per gram, and has extremely low thermal conductivities and fascinating acoustic properties due to the porous structure. The high surface area of such metal oxide aerogels provides better properties for applications such as catalysis and insulation. This in turn helps compensate for the relatively high capital cost and inconvenience of high pressure operation. The chemistry, physics and properties of materials resulting from the sol−gel process in the liquid phase have been reviewed by Gesser, Hench, Pajonk, Schubert, and co-workers.[24,54,63,64] In addition, there are comprehensive textbooks available on the physics and chemistry of sol−gel science.[56,65]

Recent developments in sol−gel technology are marked by the use of organic solvents or SCFs for synthesizing a variety of metal oxides.[66−70] However, it should be noted that, conventional organic solvents are currently used by manufacturing and processing industries on a scale of billions of kilograms per year. The fact that they play a significant role in global environmental pollution and smog formation cannot be ignored. Alternatively, since SCFs are considered to be environmentally benign,[35] and ecological credits are added to the sustainability of the sol−gel process, they offer a viable alternative.[29] Another major advantage of using SCFs as reaction media for sol−gel reactions lies in the fact that the resulting materials are readily dried after SCF venting. Such one-pot synthesis processes are attractive, as described later in this review. Additionally, sol−gel reaction kinetics can be fine-tuned using both pressure and temperature, thus allowing some difficult sol−gel reactions to take place, for example, hydrolysis and condensation of metal nitrates in SCW. Finally, although materials prepared using conventional sol−gel reactions are often amorphous (e.g., TiO_2 and ZrO_2[71,72]) many crystalline metal oxides can be readily prepared in high temperature sol−gel SCF processes. This eliminates the heat-treatment step and further simplifies the manufacturing process.[73]

2.2.1. Supercritical Carbon Dioxide. There are many benefits of using $scCO_2$ as the reaction media: CO_2 is inflammable, nontoxic, abundant and inexpensive, and it has a relatively low T_c (304.2 K) and a moderate P_c (7.375 MPa). Importantly, $scCO_2$ has already been used as an established medium for industrial-scale polymerizations, as well as food and nutrition production.[74] Generally, $scCO_2$ is a hydrophobic solvent but it possesses a large quadrupole moment and a polar C═O bond and this renders a variety of materials (e.g., with hydroxide, carbonyl or fluoride groups) soluble.[75]

The first sol−gel reactions in $scCO_2$ were reported by Tadros et al. of Sandia National Laboratories in the U.S.A. in 1996. In a batch reactor, a fluorinated anionic surfactant, $(F(CF_2CF_2)_zCH_2CH_2O)_xP(O)(ONH_4)_y$, was used to disperse water that consequently reacted with TTIP to form TiO_2 particles with diameters in the 0.1−2 μm range and with anatase crystallinity.[76] TiO_2 particles were also obtained using other surfactants in subcritical CO_2 by Johnston et al.[77,78] They investigated the electrostatic stabilization of the oxide particles by surfactants.[79] As an alternative to water, formic acid and acetic acid are miscible with $scCO_2$, and have been shown to be excellent polycondensation agents for sol−gel reactions. In 1997, Shea et al prepared monolithic SiO_2 aerogels for the first time by using formic acid reacting with TMOS in $scCO_2$.[80] Following this, Charpentier et al subsequently synthesized SiO_2, TiO_2, ZrO_2, hybrid oxides of ZrO_2−TiO_2 and Al_2O_3 aerogels with various morphologies using acetic acid reacting with the corresponding alkoxide precursors.[81−85] Among the many advantages of using formic/acetic acid instead of water for initiating the sol−gel reactions in $scCO_2$, two factors stand out: (1) water is generated in situ through esterification or dehydration from alcohols, thus moderating the hydrolysis rate

dx.doi.org/10.1021/cr2000465 | Chem. Rev. 2012, 112, 3057−3082

for Ti/Zr alkoxides; and (2) the acetate group is able to bridge many metal cations thus forming complexes which are less reactive.[86] This may facilitate self-assembly into either 1-dimensional (1-D) or 3-D nanostructures.[87,88] More metal oxides prepared via sol–gel routes in $scCO_2$ are summarized in Table 3.

Table 3. Oxide Nanomaterials Prepared by Sol–Gel Reactions in $scCO_2$ and Subcritical CO_2

products	reactor, precursor, and reagent[a]	references
Al_2O_3	batch; $Al(O^iPr)_3$; HOAc	85
SiO_2	batch; TMOS, TEOS; HOFc, HOAc	80, 82, 89, 90
SiO_2	batch; TEOS; block copolymers	36
SiO_2	batch; TEOS; surfactants + H_2O	91
TiO_2	batch/cont.; TTIP; H_2O	92–94
TiO_2	batch; $Ti(OEt)_4$/TTIP; surfactants + H_2O	76–78, 95–101
TiO_2	batch; $TiCl_4$ + TTIP; acetic anhydride	102
TiO_2	batch/semicont.; DIPBAT[b]/TTIP; H_2O/EtOH	103
TiO_2	batch; TTIP, TTBO; HOAc	83, 87
ZrO_2	batch; $Zr(O^nPr)_4$, $Zr(O^nBu)_4$; HOAc	84
ZrO_2	batch; zirconyl nitrate; surfactants + H_2O	104
Cu/Cu_2O	batch/cont.; $Cu(hfa)_2$, EtOH,	105
$Ce_{0.9}Gd_{0.1}O_{1.95}$	batch; $Ce(OAc)_3$, $Gd(OAc)_3$; H_2O	106
Al_2O_3/SiO_2	batch: $Al(O^iPr)_3$, TEOS; H_2O	107
TiO_2/SiO_2	batch: TTIP, TEOS; H_2O	108
TiO_2/SiO_2	batch: TTIP, SiO_2 alcogel; H_2O	109, 110
Fe_2O_3/TiO_2	batch: TTIP, $Fe(NO_3)_3 \bullet 9H_2O$	111
ZrO_2/TiO_2	batch; TTIP, $Zr(O^nPr)_4$; HOAc	81
Al_2O_3/carbon nanotubes	batch; $Al(NO_3)_3$	112
Eu_2O_3/carbon nanotubes	batch; $Eu(NO_3)_3$	113
Fe_2O_3/carbon nanotubes	batch; $Fe(NO_3)_3$	114
ZrO_2/carbon nanotubes	batch; $Zr(NO_3)_4$	115

[a]Type of reactors; the precursors of metal oxides; polycondensation reagent. [b]DIPBAT = diisopropoxititanium bis(acetylacetonate).

2.2.2. Supercritical Organic Solvents. In a typical sol–gel process for preparing oxide aerogels, after formation of the gel, the wet gel requires solvent exchange followed by SCF drying. This is a tedious process that requires many days to finish. In order to accelerate sol–gel reactions, Pommier et al pioneered a high temperature SCF technique for the synthesis of metal oxide particles,[116] which is also called the solvothermal method.[117–119] This method involves heating a metal alkoxide-alcohol solution in an autoclave until supercritical conditions are reached. The advantages of using supercritical organic solvents include: (1) the reaction temperature can reach a higher level than the solvents normal boiling point, thus accelerating chemical reaction rates; (2) the solubility of some inexpensive sol–gel precursors, for example, metal acetates, is much higher in polar organic solvents than in nonpolar solvents (e.g., $scCO_2$), (3) compared with SCW, supercritical alcohol is a mild reagent that does not react with metal alkoxides immediately.

For a typical high-temperature sol–gel reaction in a supercritical organic solvent, the reaction mechanism can be written as:[120]

$$ML_2 \xrightarrow{ROH} [ML(OR)(ROH)]_n + nHL \quad (2)$$

$$[ML(OR)(ROH)]_n \xrightarrow{ROH+H_2O} [M(OR)_x(OH)_{4-x}]_n + nHL \quad (3)$$

where L = acetylacetonate (acac) or hexafluoroacetylacetonate (hfa).

In the case of MgO synthesis from MgL_2, the chemical structures of the metal precursors and the intermediate compounds are as described in Scheme 2; here the coordination number of Mg is four. The solubilities of these types of materials are critical for nanoformation as described in detail later in this review. In the intermediate molecules, there are bridging $-OCH_3$ and $-OH$ groups (as evidenced by powder FTIR analysis), which can be thermally decomposed into MgO at temperatures above 723 K.[120]

Scheme 2. Similarity of the Magnesium Atom Coordination in (a) $Mg(acac)_2$, (b) Mg Acetate, and (c) Intermediate Compound Obtained in MgO Synthesis. Reproduced with Permission from ref 120. Copyright 1995 Elsevier.

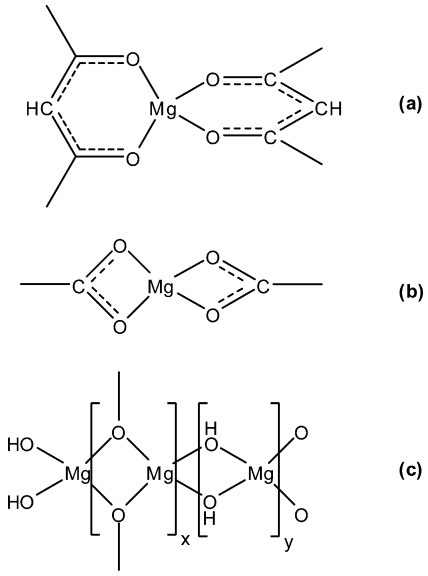

In another proposed reaction mechanism for the solvothermal process, the first step involves condensation of alcohol under high temperature and pressure, giving rise to water, which consequently reacts quickly with the metal precursor generating metal oxide particles.[121]

$$2ROH \rightleftharpoons ROR + H_2O \quad (4)$$

$$ML_2 \xrightarrow{H_2O} M(OH)_4 \rightarrow MO_2 \quad (5)$$

A comparative study was carried out by Pommier et al. of the liquid and supercritical phases of ethanol/isopropanol, using titanium alkoxides ($Ti(OC_2H_5)_4$ and $Ti(O^iC_3H_7)_4$) as precursors for the preparation of TiO_2 submicrometer particles.[117] In the supercritical ethanol process, no water was added; while in the liquid ethanol process, water was added to initialize the sol–gel reactions. The main differences found between the products prepared in the SCF and liquid ethanol process include: (1) the TiO_2 prepared in the SCF consisted of anatase crystals while that prepared in liquid ethanol was amorphous; (2) in the SCF the 20–60 nm crystallites agglomerated into 2 μm spherical spheres, while in liquid

dx.doi.org/10.1021/cr2000465 | Chem. Rev. 2012, 112, 3057–3082

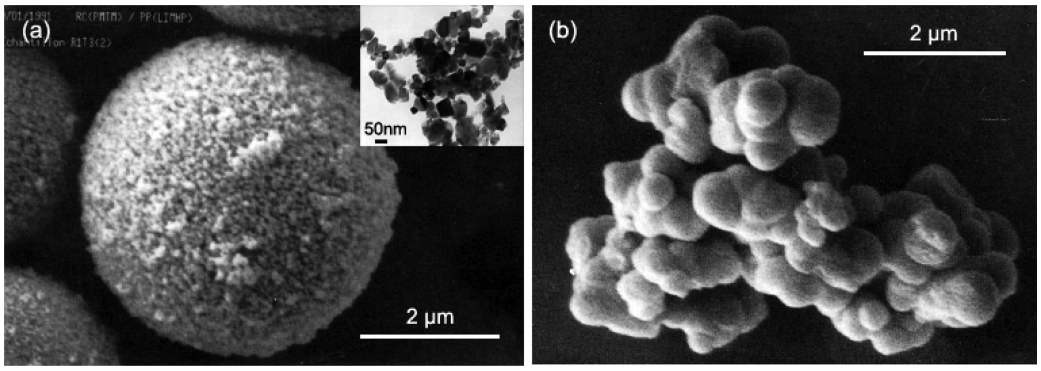

Figure 5. (a) SEM and TEM (inset) images of TiO_2 particles prepared in supercritical ethanol at 633 *K* with $Ti(O^iC_3H_7)_4$ as the precursor; (b) TiO_2 particles prepared via a sol–gel route in ethanol under ambient pressure. Reprinted with permission from ref 117. Copyright 1992 Elsevier.

ethanol the 300–700 nm amorphous spheres grew into irregular larger particles (Figure 5); (3) the specific BET surface area of the amorphous TiO_2 prepared in liquid ethanol was 150 m^2/g, while that of anatase TiO_2 prepared in the SCF was 40 m^2/g. The drop in surface area was attributed to the destruction of the micro/mesopores during the crystallization process. To make the process more feasible for commercialization, Pommier et al designed a continuous reactor using the supercritical alcohol process for production of TiO_2. The relevant reactor processes will be described later in this review. In Table 4, metal oxide aerogels prepared in supercritical organic solvents are summarized.

Table 4. Metal Oxides Prepared by the Sol–Gel Reactions in Supercritical Organic Solvents

products	reactor, supercritical fluid, and precursor[a]	refs
Cr_2O_3	semicont./MeOH/$Cr(acac)_3$/$Cr(OAc)_3$	123
MgO	batch/semi-cont.; supercrit. MeOH/EtOH–CO_2; $Mg(acac)_2$/$Mg(hfa)_2$/$Mg(OMe)_2$	120, 124
TiO_2	batch; supercrit. EtOH/^{i}PrOH; $Ti(OEt)_4$/TTIP	117, 125–127
TiO_2	cont.; supercrit. ^{i}PrOH, ^{n}PrOH; TTIP, $TiCl_4$	122, 128
$BaTiO_3$	cont./semicont.; supercrit. EtOH, ^{i}PrOH; $Ba(O^iPr)_2$, TTIP, $BaTi(O^iPr)_6$	129–131
$MgAl_2O_4$	batch; supercrit. EtOH; $Mg[Al(OC_4H_9)_4]_2$/$Mg[Al(OC_2H_5)_4]_2$	116, 132
$Y_3Al_5O_{12}$	cont.; supercrit. EtOH-H_2O; $Al(acac)_3$/$Al(OAc)_3$, $Y(OAc)_3$	133
$ZnFe_2O_4$	batch; supercrit. MeOH; $Zn(OAc)_2$, $Fe(acac)_3$ + H_2O	134
Cr_2O_3/carbon nanotubes	batch; supercrit. EtOH; $Cr(NO_3)_3{\cdot}9H_2O$	135
TiO_2/carbon nanotubes	batch; supercrit. EtOH; TTIP	136
RuO_2/carbon nanotubes	batch; supercrit. diethyl amine; $RuCl_3{\cdot}9H_2O$	137

[a]Type of reactors; type of supercritical fluids; the precursors of metal oxides.

2.2.3. Supercritical Water. Sol–gel reactions for oxide synthesis in supercritical water are also called hydrothermal synthesis in supercritical water (HTS-SCW).[43] It should be noted that hydrothermal synthesis often refers to using a high concentration of alkaline aqueous solution at elevated temperatures at ambient pressures far below the critical pressure.[138] This particular type of reaction is not covered in this review. SCW is not only an excellent reaction media for a number of reactions,[139] but it can also act as a reagent that can quickly react with metal alkoxides or even salts to form metal oxides. The rapid reaction kinetics in SCW makes it possible to prepare metal oxide nanoparticles using continuous reactors, which is more attractive for industrial scale production. Other advantages of using SCW include: (1) the tunable dielectric constant of water (Figure 6), provides an extra parameter for controlling the solubility of the solutes in addition to the SCF density; (2) the high crystallinity of the metal oxide products formed, and (3) lower temperatures for the formation of certain crystals in SCW, for example, γ- and α-Al_2O_3 is formed at 573 and 673 K in SCW, respectively.[140] This is significantly lower than the crystallization temperature of over 973 K required for γ-Al_2O_3 and over 1273 K for α-Al_2O_3 under ambient pressure. As described by Poliakoff et al,[141] as for other sol–gel reactions, a typical HTS-SCW process involves the hydrolysis of a metal precursor with H_2O and subsequently a condensation step that results in the formation of oxo bonds in the metal oxide. This is described by

$$\text{hydrolysis: } ML_x + xOH^- \rightleftharpoons M(OH)_x + xL^- \quad (6)$$

$$\text{condensation: } M(OH)_x \rightleftharpoons MO_{x/2} + \frac{x}{2}H_2O \quad (7)$$

where L = NO_3^-, $CH_3CO_2^-$, M = Ce, Zr, Ti, Cu, Y, In, Pa, Rh, etc.[142]

The drawbacks of SCW include the high temperature/pressure (T_c = 647.3K and P_c = 22.1 MPa), as well as problems caused by the corrosion of the high pressure apparatus, which

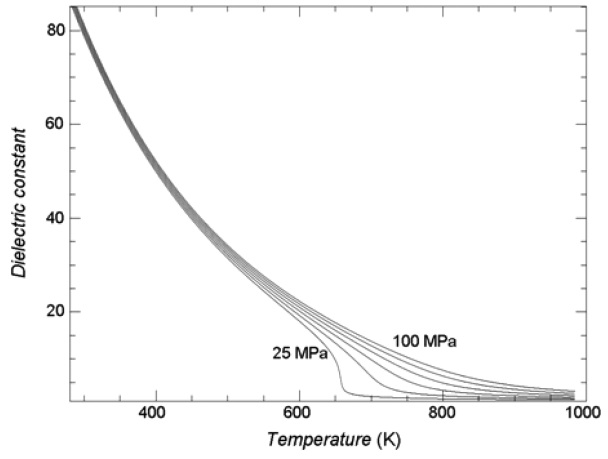

Figure 6. Dielectric constant of water. The plot was obtained using the NIST Standard Reference Database Version 9.0.

dx.doi.org/10.1021/cr2000465 | *Chem. Rev.* 2012, 112, 3057–3082

Table 5. Metal Oxides Prepared by the HTS-SCW Method

products	reactor and precursor[a]	references
AlO(OH)	batch; $Al(NO_3)_3$	22, 143−146
CeO_2	cont.; $Ce(NO_3)_4$ or $Ce(OAc)_4$	22, 141, 142, 147, 148
Co_3O_4	cont.; $Co(NO_3)_2$	143, 149
Cu_2O	batch; $Cu(CH_3CO_2)_2$	150
CuO	batch; $Cu(NO_3)_2$	150, 151
Fe_2O_3	batch; $Fe(NO_3)_3$	152
Fe_2O_3	cont.; $Fe(NH_4)_2H(C_6H_5O_7)_2$/ $Fe(NO_3)_3$	143, 149, 151, 153
Fe_3O_4	cont.; $Fe(NO_3)_3/Fe_2(SO_4)_3/FeCl_2/Fe(OAc)_2$	143, 154, 155
NiO	cont.; $Ni(NO_3)_2$	143, 151
TiO_2	batch/cont.; $TiSO_4/TiCl_4$/TTIP/$Ti(NO_3)_4$ or $Ti(OAc)_4$	22, 141−143, 156
ZnO	cont.; $Zn(OAc)_2/Zn(NO_3)_2$	141, 157−159
ZrO_2	cont.; $ZrOCl_2/Zr(NO_3)_4$ $Zr(OAc)_4$	141−143, 147, 151
BaO/Fe_2O_3	batch/cont.; Fe(III)/$Ba(NO_3)_2$	22, 160
core Fe_2O_3/shell SiO_2	batch; Fe_2O_3/TMOS	161
Fe_2O_3/In_2O_3	batch; $Fe(NO_3)_3$, $In(NO_3)_3$	162
CuO/ZnO	cont.; N/A	141
$Ce_{1-x}Zr_xO_2$	cont.; Ce/$Zr(NO_3)_4$ or $Zr(OAc)_4/(NH_4)_2[Ce(NO_3)_6]$	142, 147
$CoFe_2O_4$	cont.; Co(II) $(NO_3)_2$; $Fe(NO_3)_3$	154, 163
La_2CuO_4	cont.; La(III)/$Cu(NO_3)_2$ or $Cu(OAc)_2$	142, 164
$NiFe_2O_4$	cont.; Fe(II)/$Ni(OAc)_2$	154
$ZnFe_2O_4$	cont.; Fe(II)/$Zn(OAc)_2$	154
Zn_2SiO_4:Mn^{2+}(ZSM)	batch; ZnC_2O_4/MnC_2O_4, am. SiO_2	165
$Ca_{0.8}Sr_{0.2}Ti_{1-x}Fe_xO_{3-\delta}$ (x = 0.1−0.3)	cont.; $Ca(NO_3)_2$, $Sr(NO_3)_2$, $Fe(NO_3)_3$, TiO_2 sols	166
$(Y_{2.7}Tb_{0.3})Al_5O_{12}$	cont.; $Tb(NO_3)_3$, $Y(NO_3)_3$, $Al(NO_3)_3$	167

[a]Type of reactors; the precursors of metal oxides.

may increase the capital cost for more expensive anticorrosive materials, for example, Hastelloy. More metal oxides prepared in SCW are summarized in Table 5.

3. FORMATION OF NANOSTRUCTURES IN SUPERCRITICAL FLUIDS

As summarized by Heller and Brinker et al,[56,168] the formation of different nanostructures (e.g., 1-D rods, 2-D plates. and spheres) results from the building blocks of colloidal particles (sols) in solvents. Colloids and solvent are susceptible to phase separation and colloids segregate into concentrated regions surrounded by the bulk fluid. These concentrated regions are called coacervates. When the colloids are regularly oriented they are referred to as tactoids, which can change irreversibly into rigid structures called crystalloids after either drying or reduction of the repulsive barrier between the colloids. Finally, aggregation of crystalloids results in the formation of flocks which can gel under appropriate conditions (Figure 7).

Since the growth of the sol particles increases the viscosity of the solution during the course of the sol−gel process, the formation of the gel, or the gelation process, can be conveniently studied by measuring and modeling the viscosity.[169,170] Aymonier et al developed a model for particle growth in SCFs based on a two step mechanism: the coalescence and aggregation of monodispersed primary particles. The model is dedicated to predicting the aggregate size in the autoclave as a function of the operation parameters, for example, pressure, temperature, precursor concentration, and residence time.[171] However, this model needs validation for metal oxide growth under different conditions.

Since the physical and chemical properties of metal oxide nanomaterials are a function of their morphologies, one of the primary goals in the emerging field of direct sol−gel synthesis and processing, is to tune both the shape and size of the resulting metal oxides. In the case of direct sol−gel chemistry, this goal can be achieved by tuning synthesis parameters such as temperature, pressure, concentration of materials, and judicious choice of starting materials and solvents.

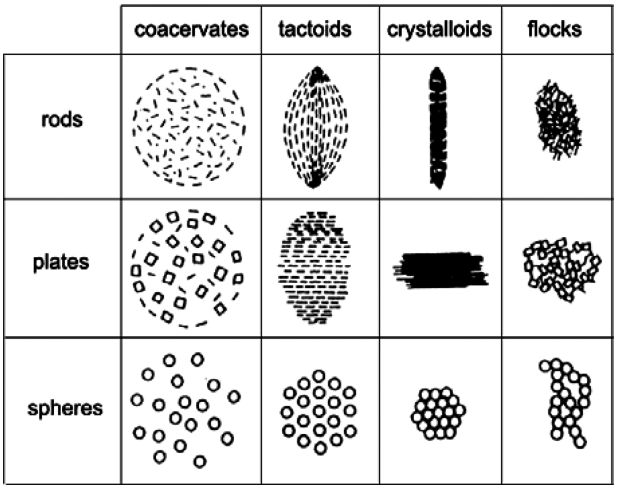

Figure 7. Principal types of nanostructures derived from colloids. Reproduced with permission from ref 56. Copyright 1990 Academic Press, Inc.

3.1. Monoliths

Monolithic aerogels are constituted of a 3-D structure of suitable porous materials that are in turn composed of aggregated particulate aerosols. Monolithic aerogels of SiO_2, Al_2O_3, and TiO_2 are of interest for applications in catalysis, insulation materials, and monolithic chromatography columns for protein separation.[172,173] As described earlier, because of shrinkage and cracking during the drying of the wet gel under ambient pressure, supercritical drying has been widely used for

dx.doi.org/10.1021/cr2000465 | Chem. Rev. 2012, 112, 3057−3082

preparing crack-free monoliths with high porosity.[56] Within this context, therefore, it is attractive to use the direct sol−gel process in SCFs to prepare monolithic aerogels. This simplifies the synthesis procedures compared to more conventional sol−gel methods. Formation of an aerogel monolith needs sufficient concentration of starting materials, and enough reaction time for the gelation and aging processes. As the predecessor of the aerogel, the gel is considered as forming from the aggregation of the particulate sols into a continuous 3-D solid network,[56] which fills up the whole autoclave. Using alkoxides as precursors and formic or acetic acid as the polycondensation reagent, SiO_2, TiO_2, and ZrO_2 monolithic aerogels were prepared in $scCO_2$.[80,84,87] It is noteworthy that monoliths have been prepared in low temperature $scCO_2$, not only in high temperature SCW or supercritical organic solvents. Gelation is a slow process and it requires days of aging to make the solid network strong, hence a low temperature is favorable for monolith formation. On the other hand, high temperatures accelerate the hydrolysis and condensation reactions which in turn enhance particulate formation.

To enhance the sol−gel reactions of TMOS in $scCO_2$, formic acid has been used as an alternative to water as the polycondensation reagent. Results showed that when the concentration of TMOS was in the range of 1.9−2.3 mol/L, successful gelation occurred and after aging for 12−18 h, the procedure involved CO_2 venting.[80] Figure 8 shows the SiO_2 aerogel monolith obtained, where the cylindrical shape is a result of the interior geometry of the reactor. Using TMOS and ethyltrimethyloxysilane (ETMOS) as precursors, the previously packed SiO_2 particles in a chromatography column were successfully "sol-gel bonded" to form monolithic SiO_2. The in situ-formed gel was prepared in $scCO_2$, and this promoted the mechanical strength and the separation performance of the resulting columns.[174] Recently, TiO_2 monolithic aerogels formed inside stainless steel tubing using the sol−gel route in $scCO_2$ were used for chromatography columns (Figure 9).[175]

Figure 8. Photograph of monolithic SiO_2 aerogel (1 cm × 3.2 cm) prepared by sol−gel reactions of TMOS reacting with formic acid in $scCO_2$. Reprinted with permission from ref 80. Copyright 1997 American Chemical Society.

The mechanism of the reaction of silicon alkoxides with carboxylic acid in conventional organic solvents has been studied by Sharp.[176] The first two steps are substitution and esterification reactions:

$$\equiv Si{-}OR + R'COOH \rightleftharpoons \equiv Si{-}OOCR' + HOR \quad (8)$$

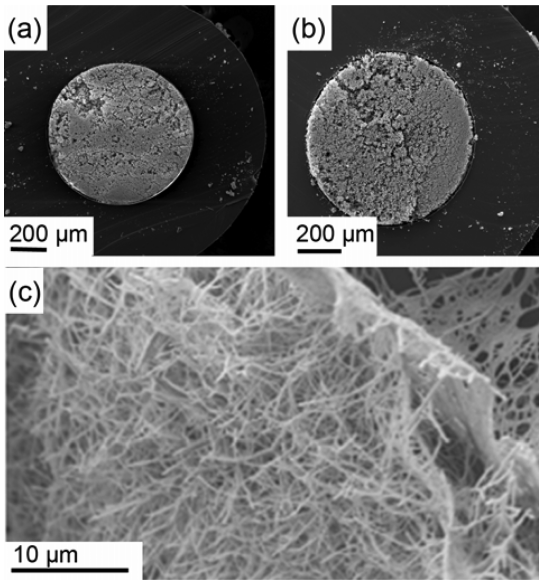

Figure 9. Cross sections of a column filled with monolithic TiO_2 (a and b). The higher magnification SEM image shows the TiO_2 nanofibrous structure (c). Reprinted with permission from ref 175. Copyright 2010 Wiley-VCH.

$$R'COOH + HOR \rightleftharpoons H_2O + ROOCR' \quad (9)$$

The generated water formed as a result of the esterification step is able to hydrolyze the alkoxides. However, the esterification step is inherently slow,[34] and thus it is difficult to explain the fast sol−gel reactions as observed in $scCO_2$.[177] To study the reaction mechanism, GC-MS and NMR were used to analyze the intermediates that showed the presence of bridging −OR groups such as $C_7H_{21}O_7Si_2^+$ and $(C_6H_{18}O_9Si_3)^+$.[178] On the basis of the GC-MS and NMR results, the formation of a methoxyl bridging structure and the subsequent oxolation reactions can be written as follows:

$$\equiv Si{-}OMe + HOAc \rightleftharpoons \equiv Si{-}OAc + MeOH \quad (10)$$

$$\equiv Si{-}OAc + MeO{-}Si\equiv \rightleftharpoons [\equiv Si{-}OMe{-}Si\equiv]^+ + OAc^- \quad (11)$$

$$[\equiv Si{-}OMe{-}Si\equiv]^+ + HOAc \rightleftharpoons \equiv Si{-}O{-}Si\equiv + MeOAc + H^+ \quad (12)$$

$$[\equiv Si{-}OMe{-}Si\equiv]^+ + H_2O \rightleftharpoons \equiv Si{-}O{-}Si\equiv + MeOH + H^+ \quad (13)$$

The new mechanism circumvents the slow esterification reaction pathway. Thus, the substitution−condensation pathway (eqs 10−13) may play an important role in the polycondensation of silicon alkoxides with acetic acid in $scCO_2$.[178]

Because of the zero surface tension of the SCF, the solid network of the oxides and the meso-/microprores of the gel are maintained during the SCF drying process. Consequently, this results in a low apparent density, and a high specific surface area and pore volume of the aerogel products. These monolithic aerogel properties are especially attractive for applications as catalyst supports and insulation materials. In Tables 6 and 7 are listed typical densities, specific surface areas and pore volumes of several oxide aerogels prepared by either SCF drying or

dx.doi.org/10.1021/cr2000465 | Chem. Rev. 2012, 112, 3057−3082

Table 6. Apparent Densities of Some Aerogels

aerogel	apparent density	calcination temperature (K)	ref
SiO_2	0.271−0.423	N/A	181
SiO_2	0.07−0.17	N/A	182
SiO_2	0.085−0.389	N/A	183
SiO_2	0.04−0.27	N/A	184
TiO_2−SiO_2	0.31−0.64	573	185
lanthanide-doped SiO_2−Al_2O_3	0.15−0.45	523	186
Al_2O_3	0.02−0.16	N/A	184
TiO_2	0.2−1.2	N/A	184
TiO_2	0.12−0.20	653	87
ZrO_2	0.02−0.50	N/A	184

direct sol−gel reactions in SCFs. Of these aerogels, SiO_2 and Al_2O_3 exhibited the highest specific BET surface area, for example, over 1000 m^2/g for SiO_2 and 600 m^2/g for Al_2O_3. For TiO_2 and ZrO_2, the BET surface areas are normally below 200 and 100 m^2/g, respectively. Even though these oxides are well-known for their thermal stability, it is noteworthy that the surface area is affected by the calcination temperature: a higher temperature often results in lower surface areas because of the resultant sintering of the oxide using the high temperature treatment. The sintering phenomenon has been explained by condensation of water from the hydroxide groups on adjacent oxide particles (Figure 10).[179] From a practical perspective, better thermal stability can be achieved by the addition of small amounts (<3 wt %) of other metal oxides such as lanthanum or yttrium oxides.[180]

3.2. Spherical Particles

Because of their low surface area and interfacial energy per volume, spheres and pseudospheres are the most common shape formed of the different possible nanomaterial geometries. Numerous reports are documented for the synthesis of metal and silicon oxide spherical particles in SCFs.[82,91,92,100,188−190] For instance, SiO_2 spherical particles, with a relatively narrow particle size distribution, were obtained via the sol−gel reactions of TMOS reacting with varying amounts of water (molar ratio H_2O/TMOS = 2, 4, 8) in supercritical acetone.[89] Nanoparticulate ferrites MFe_2O_4 (M = Co, Ni, Zn, and Fe), a ceramic material usually containing iron and with applications as magnetic components and in microelectronics, have been prepared in a continuous reactor using metal acetates in H_2O at 473−673 K and 25 MPa.[154]

Owing to its high thermal stability and oxidation resistance, yttrium aluminum garnet (YAG, $Y_3Al_5O_{12}$) has attracted much attention and has been synthesized in SCFs. For instance,

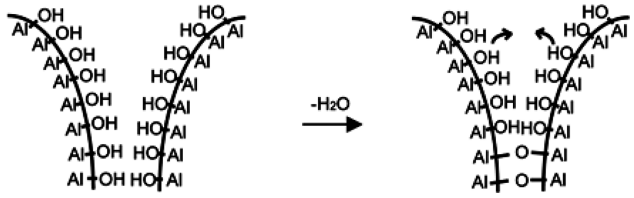

Figure 10. Model representing surface dehydration from the contact region of two adjacent particles that results in the alumina sintering. Reproduced with permission from ref 179. Copyright 1996 Elsevier.

Lester et al prepared $Y_3Al_5O_{12}$ nanoparticles by using yttrium and aluminum acetates/acetylacetonate as the precursors and reacting them with SCW in the presence of EtOH (Figure 11).[133]

SiO_2 hollow spheres, which are more challenging to synthesize, were first reported by Mokaya and Paliakoff et al who used a CO_2-in-water emulsion templating method.[91,190] By using block-copolymers such as poly(ethylene oxide)-*b*-poly(propylene oxide)-*b*-poly(ethylene oxide) (PEO-PPO-PEO) that can form micelles in water, the CO_2 phase was stabilized within the core of the micelles. On the basis of its high solubility in $scCO_2$, the precursor TEOS remains in the CO_2 phase and slowly reacts with water at the micelle interface. This eventually results in a hollow SiO_2 structure with a diameter of a few micrometers (Figure 12).[190] Following this idea, hollow

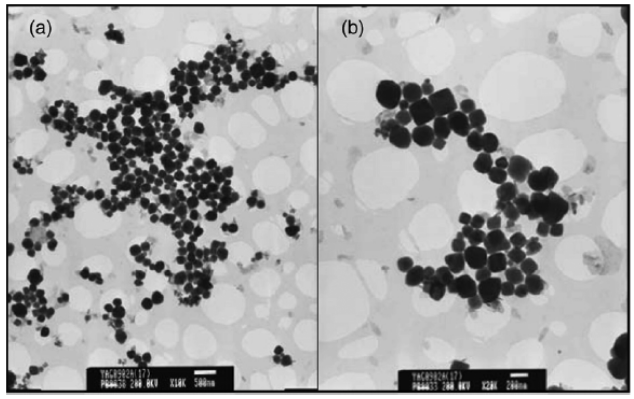

Figure 11. TEM of YAG particles produced by HTS-SCW using Al acetate and Y acetate as precursors, with 60 vol % EtOH in H_2O at 658 K and 24 MPa. Scale bars: (a) 500 nm and (b) 200 nm. Reprinted with permission from ref 133. Copyright 2007 Elsevier.

submicrometer SiO_2 and hollow Ti-containing SiO_2 were prepared in $scCO_2$ either by using reverse micelles (water in oil)[189] or by using another surfactant, cetyltrimethyl-ammo-

Table 7. BET Surface Area and Pore Volume of Some Aerogels

aerogel	S_{BET} [a] (m^2/g)	V_{pore} [b] (cm^3/g)	crystalline	calcination temperature (K)	ref
SiO_2	162−1004	0.30−1.81	N/A	N/A	184
SiO_2	197−739		am.[c]	N/A	80
Al_2O_3	26−464	0.22−0.95	am., $\delta + \eta$	673−1273	184
TiO_2	105−270		anatase	653	83
TiO_2	~200	~0.65	anatase	773	71
ZrO_2	96−145	0.32−0.49	N/A	773	187
ZrO_2	101	0.051	tetragonal	673	84
ZrO_2	51−76	0.045−0.24	monoclinic	773	84

[a]BET surface area. [b]Total pore volume per gram measured using N_2 at 77 K. [c]Amorphous.

dx.doi.org/10.1021/cr2000465 | *Chem. Rev.* 2012, 112, 3057−3082

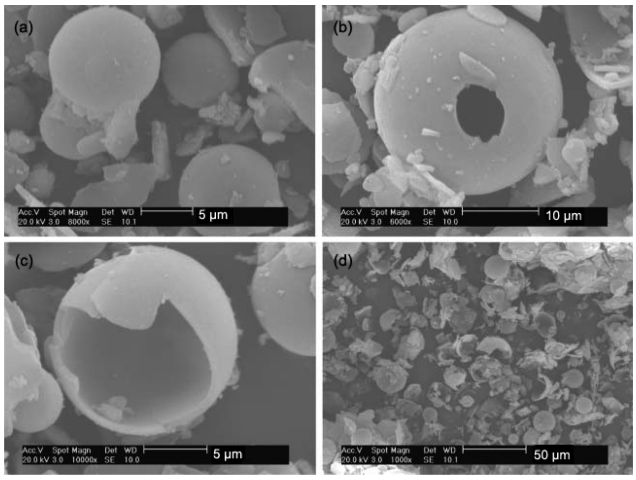

Figure 12. SEM images of calcined SiO_2 hollow spheres prepared in $scCO_2$ with the aid of PEO-PPO-PEO block copolymers. Reproduced with permission from ref 190. Copyright 2005 Royal Society of Chemistry.

nium bromide (CTAB) (Figure 13).[188] A recent report shows that the shells of the hollow SiO_2 sphere exhibit ordered mesopores when the sol–gel process took place in water/heptane/CTAB nanoemulsions in compressed CO_2.[191]

3.3. 1-D Oxides

The family of 1-D nanostructured materials includes nanoscale wires/fibers, tubes, rods and belts. Even though 1-D nanomaterials can be traced back to 1921 when Hg nanofibers were prepared by Volmer and Esterman,[192] they only began to attract significant attention some seventy years later after Iijima reported the discovery of carbon nanotubes.[193] Interest in this family of nanomaterials currently lies in their unique mechanical, optical and electronic properties. 1-D nanomaterials of metals, alloys, and metal oxides, have been comprehensively reviewed by both Xia and Yang et al,[194] and Seal et al.[195] Among the strategies summarized by Xia and Yang et al, the three methods most commonly used for synthesizing a number of 1-D metal oxide nanostructures via sol–gel reactions in SCFs are: (1) anisotropic crystallization of linear macromolecules; (2) 1-D growth using either templates such as channels in mesoporous materials or premade 1-D structures and self-assembled structures of surfactants, followed by removal of the templates by corrosion or heat treatment; and (3) 1-D growth from the vapor or liquid phase through control of the supersaturation. This includes direct/indirect vapor-phase, vapor–liquid–solid (VLS), solution-liquid–solid (SLS) and solvothermal methods. Some examples are: TiO_2 and Al_2O_3 nanofibers, and hybrid oxide ZrO_2/TiO_2 nanotubes prepared using the anisotropic crystallization (strategy 1);[81,83,85] TiO_2 nanotubes and nanofibers manipulated using the templating method (strategy 2);[95,196,197] and ZnO nanorods which were synthesized using the solvothermal method (strategy 3).[159]

Compared with spherical particles that are favored by a reduced surface area, the formation of 1-D oxide particulates is less common when sol–gel reactions are employed. Using $scCO_2$ as the solvent, TTIP and TTBO as the precursors and HOAc as the polycondensation reagent, randomly oriented nanofibers or nanospheres of TiO_2 aerogels were successfully produced (Figure 14).[83] It was observed that a high acid ratio

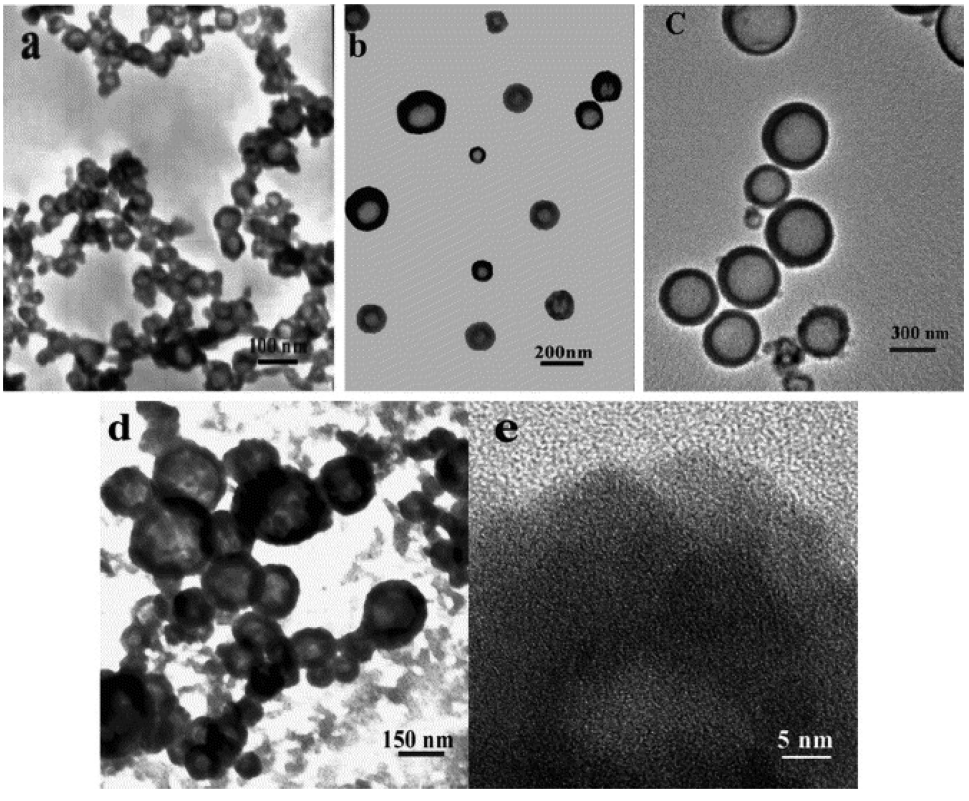

Figure 13. TEM images of hollow SiO_2 spheres. The synthesis conditions: V_{TEOS} = 2.0 mL, reaction temperature = 313.2 K, (a) [CTAB] = 0.003 mol/L, P = 9.78 MPa; (b) [CTAB] = 0.003 mol/L, P = 8.69 MPa; (c) [CTAB] = 0.003 mol/L, P = 0.54 MPa; (d) [CTAB] = 0.03 mol/L, P = 8.69 MPa; (e) HRTEM image of a hollow SiO_2 sphere corresponding to figure (c). Reprinted with permission from ref 188. Copyright 2007 Elsevier.

dx.doi.org/10.1021/cr2000465 | *Chem. Rev.* 2012, 112, 3057–3082

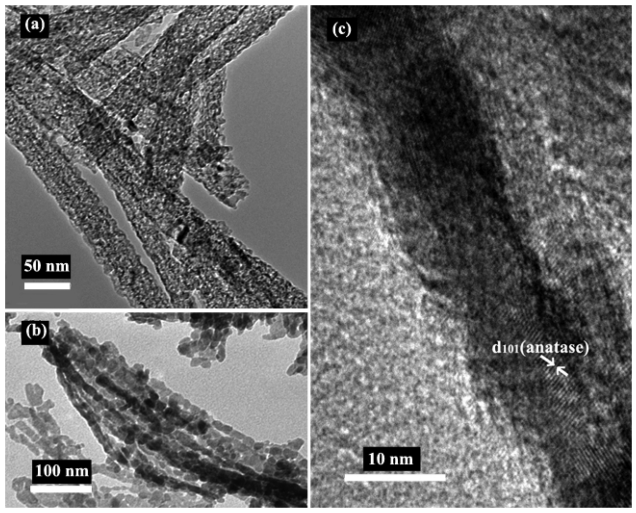

Figure 14. TEM images of TiO_2 nanofibers prepared in $scCO_2$ at 41.4 MPa and 333.2 K and calcined at 653 K, with a HOAc/TTIP molar ratio of 5.5 (a) and 4.1 (b, c). The *d*-spacing of 0.35 nm in the HRTEM image reveals the (101) plane of anatase within the fiber. Reprinted with permission from ref 83. Copyright 2005 American Chemical Society.

HOAc/TTIP (*R*) facilitates formation of the nanofibers (10–40 nm). Using a similar approach, the hybrid oxide nanotubes of ZrO_2/TiO_2 were also prepared in $scCO_2$. Here the molar ratios of Zr/Ti and HOAc/alkoxides were 1:9 and 5.0–6.0, respectively (Figure 15).[81] Also, using aluminum isopropoxide

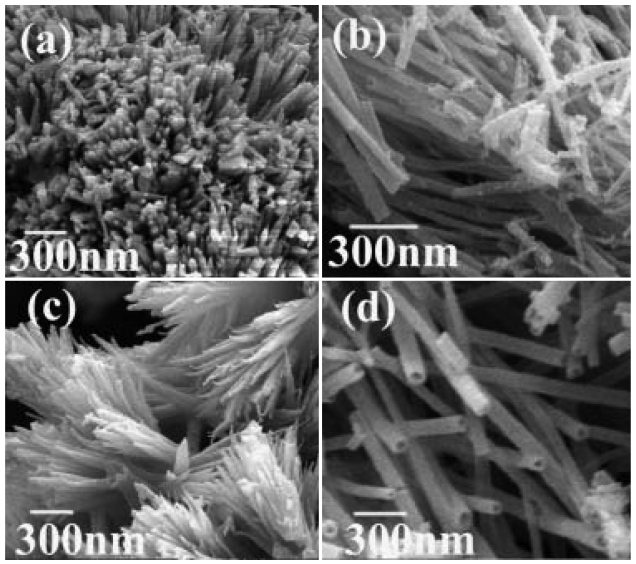

Figure 15. SEM of ZrO_2/TiO_2 (Zr/Ti = 1:9) nanotubes produced in $scCO_2$. HOAc/alkoxides molar ratio = 5.0–6.0, reaction temperature = 60 °C, and pressure = 34.5–41.4 MPa. Reproduced with permission from ref 81. Copyright 2008 Wiley-VCH.

and reacting it with acetic acid, Al_2O_3 nanofibers were synthesized in the following forms: $[Al(OH)(CH_3CO_2)_2]_m$ (as-prepared), γ and δ-Al_2O_3 after calcination at 1073 *K*, as well as γ, δ, α and θ-Al_2O_3 at 1323 *K*.[85] The advantages of this technique include the mild reaction conditions, high yields, high productivity, and uniform nanofiber dimensions; the disadvantage is the longer reaction time required for nanofiber formation (in the time frame of tens of hours) vs the SCW technique (less than one second).

Understanding the mechanism of nanofiber formation is essential for tuning the metal oxide nanostructure morphology. Much effort has been made to study the mechanism of nanofiber formation by examining the intermediates of the sol–gel reactions of TTIP with acetic acid in $scCO_2$ and n-heptane by means of in situ ATR-FTIR,[87] electrospray ionization mass spectrometry (ESI-MS),[88] and single crystal X-ray diffraction.[198] Also, "as-prepared" aerogels were analyzed using powder FTIR and thermal analytical techniques such as DSC and TGA.[87] According to single crystal X-ray diffraction studies of crystals prepared in $scCO_2$, the reactions of TTIP and acetic acid produced a hexanuclear titanium acetate complex, $Ti_6O_6(OAc)_6(O^iPr)_6$, when the molar ratio of HOAc/TTIP (*R*) was 1.33. When *R* was higher (e.g., 5.5), the formation of $Ti_6O_6(OAc)_6(O^iPr)_6$ in $scCO_2$ and heptanes was confirmed by in situ IR spectra after deconvolution;[177] and ESI-MS analysis,[88] respectively. The step reactions of the sol–gel process can thus be written as

$$Ti(O^iPr)_4 + nAcOH \rightleftharpoons Ti(O^iPr)_{4-n}(OAc)_n + n^iPrOH \quad (14)$$

$$AcOH + {}^iPrOH \rightleftharpoons {}^iPrOAc + H_2O \quad (15)$$

$$6Ti(O^iPr)_4 + 18AcOH \rightleftharpoons Ti_6O_6(OAc)_6(O^iPr)_6 + 6^iPrOH + 12^iPrOAc + 6H_2O \quad (16)$$

$$Ti_6O_6(OAc)_6(O^iPr)_6 + nH_2O \rightleftharpoons Ti_6O_6(OAc)_6(O^iPr)_{6-n}(OH)_n + n^iPrOH \quad (17)$$

$$mTi_6O_6(OAc)_6(OH)_6 \rightleftharpoons [Ti_6O_9(OAc)_6]_m + 3mH_2O \quad (18)$$

The in situ-generated water will react with acetate-substituted TTIP and form $Ti_6O_6(OAc)_6(O^iPr)_6$, which has the crystal structure shown in Figure 16. In this hexanuclear structure, while the six bridging acetate groups are inert, the six dangling isopropoxide groups are active and able to react with water to form hydroxide groups in the axial direction. The condensation of this hexanuclear complex leads to the formation of 1-D macromolecules (or sols). These eventually form nanofibers via a coacervate and tactoid pathway.[87,88] This proposed model of TiO_2 nanofiber formation is further supported by thermal analysis with the TGA results showing that the weight loss from 473 to 773 *K* was proportional to the removal of organic groups from the $[Ti_6O_9(OAc)_6]_m$ macromolecule.

Similar to TiO_2 nanofiber formation, the anisotropic crystallization of linear macromolecules of $[Al_2(OH)_2(CH_3CO_2)_4]_m$ in $scCO_2$, as seen in Scheme 3, is believed to facilitate the fibrous growth of Al_2O_3 aerogel. Supporting analytical evidence includes IR, thermal analysis, and XPS results. The as-prepared products of TiO_2 and Al_2O_3 aerogels have yet to be examined using synchrotron powder XRD, which may provide more detailed information about the spatial arrangement of the linear macromolecules inside the fibers.

The formation of ZrO_2/TiO_2 hybrid oxide nanotubes again shows the feasibility of using the sol–gel technique in SCF for making 1-D nanostructures. Here Zr and Ti alkoxides (Zr/Ti

dx.doi.org/10.1021/cr2000465 | *Chem. Rev.* 2012, 112, 3057–3082

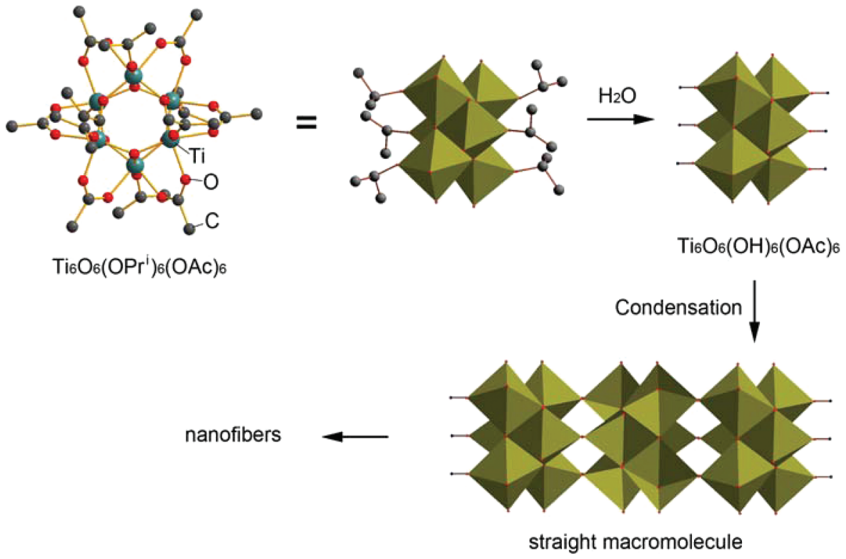

Figure 16. Molecular structure of $Ti_6O_6(OAc)_6(O^iPr)_6$, and the schematic formation of the straight macromolecule and nanofibers. (Reprinted with permission from ref 177. Copyright 2008 American Chemical Society.

Scheme 3. Schematic Diagram of the Structure of the Linear Macromolecule with a Repeating Unit of $Al_2(OH)_2(CH_3CO_2)_4$ (Ti = Blue, O = Red, C = Brown, H = Purple)

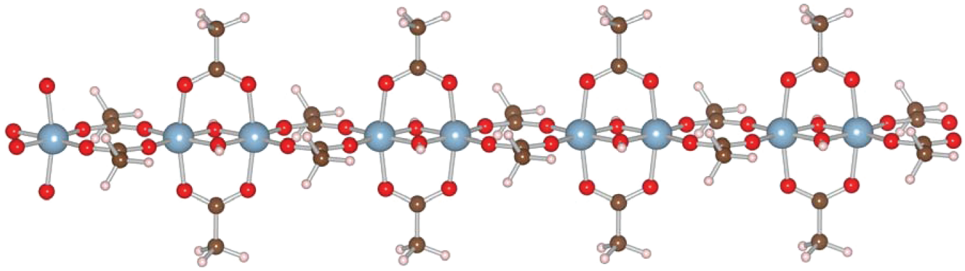

molar ratio was 1:9) were reacted with acetic acid. To explain the formation of the tubular structure, a nanosheet-bending mechanism was proposed. The sheet is formed by anisotropic growth from the triclinic crystal of the hexanuclear complexes $[Ti_4Zr_2(C_2H_3O_2)_{10}(C_3H_7O)_6O_4]$,[199] along one plane of the unit cell.[81,200] However, more characterization studies are necessary for a better understanding of the nanotube formation mechanism.

Using $Zn(NO_3)_2$ as a precursor, ZnO nanorods with diameters of ~40−100 nm and lengths of ~230−290 nm in SCW at 673 K and 30 MPa were obtained.[159] It was found that nanorods were only formed by manipulating a relatively low saturation degree of the metal oxide crystallites; otherwise spheres were formed. The production of ZnO was carried out in a continuous reactor with a residence time of 0.1 s, which makes this technique competitive for potential commercialization.

To date, the 1-D oxides formed via sol−gel reactions in SCFs are limited to disoriented 1-D structures. For their application as semiconductors such as in solar cells, it is desirable to have oxide arrays grown from the electrode surface.[10] This remains a challenge for self-assembly sol−gel reactions in SCFs.

3.4. Aerogel Membranes

With a 2-D structure composed of porous materials, an aerogel membrane consists of a layer of aggregated particulate aerosols, with a broad range of applications as optical, thermal, acoustic and electronic materials.[56] The major advantages of using SCFs as sol−gel media for the preparation of the oxide membranes include: (1) suitable wetting of the substrate surface to facilitate, with less void space, the anchoring of the oxide particles to the surface, (2) zero interfacial tension during the drying process which facilitates better film formation with less cracks and peeling, and (3) pore expansion within the membrane that is particularly beneficial for separation and catalysis applications of such membranes.

A SiO_2 film with a thickness of 1 μm was synthesized in $scCO_2$ by reacting Si alkoxides with water-wetted silicon wafers; but the properties of the resulting materials were not fully described.[201] To prepare mesoporous SiO_2 films with 1-D hexagonal closed-packed pore structures, sol−gel processing of TEOS was conducted in $scCO_2$ and subcritical CO_2 under the control of the cationic fluorinated surfactants, that is, 1-(3,3,4,4,5,5,6,6,7,7,8,8,8-tridecafluoro-octyl)pyridinium chloride (HFOPC), 1-(3,3,4,4,5,5,6,6,7,8,8,8-dodecafluoro-7-trifluoromethyl-octyl)pyridinium chloride (HFDoMePc), and 1-(3,3,4,4,5,5,6,6,7,7,8,8,9,9,10,10,10-heptadecafluoro-decyl)-pyridinium chloride (HFDePc).[202] For comparison, similar synthesis were also conducted in ethanol solution in order to examine the solvent effects. As shown in (Figure 17), an increase in the *d*-spacing and pore diameter of the material was obtained when CO_2 was used. This may increase its potential applications for chromatography and electrodes.

For potential applications in catalytic membranes and electrochemical devices, $Ce_{0.9}Gd_{0.1}O_{1.95}$ membranes were prepared in a supercritical mixture of $^iPrOH/CO_2$ (volume

dx.doi.org/10.1021/cr2000465 | *Chem. Rev.* 2012, 112, 3057−3082

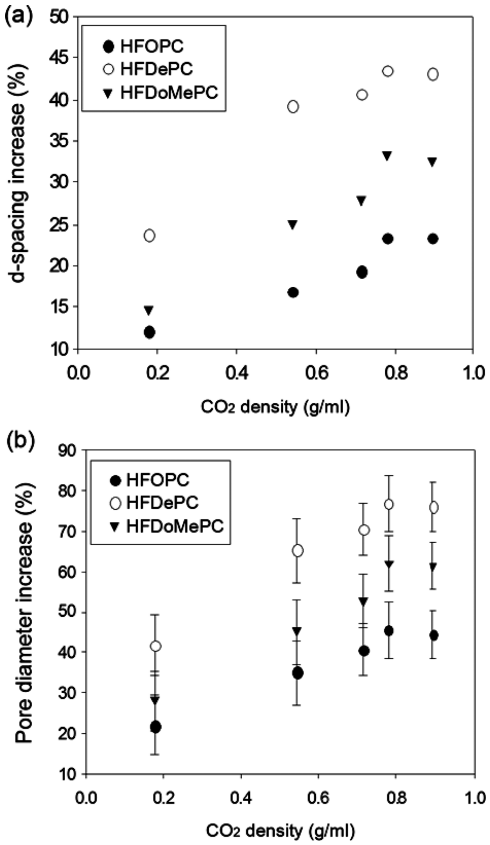

Figure 17. Percentage increase in (a) *d*-spacing and (b) pore diameter of thin films processed in CO_2 relative to unprocessed films as a function of the CO_2 density. Reprinted with permission from ref 202. Copyright 2007 American Chemical Society.

ratio = 4:1) using the sol–gel reactions of cerium acetate and gadolinium acetate with water, at 30 MPa and 150–300 °C.[106] Figure 18 shows the schematic and SEM images of the hybrid metal oxide membrane formed on top of porous α-Al_2O_3.

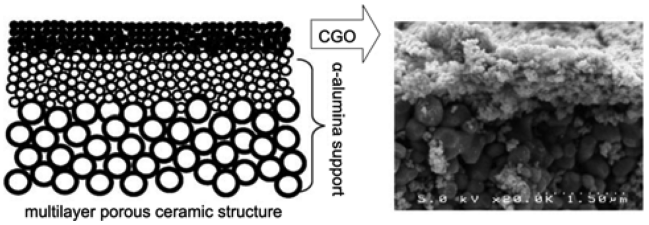

Figure 18. (a) Schematic and (b) the corresponding SEM image of α-Al_2O_3 supported $Ce_{0.9}Gd_{0.1}O_{1.95}$ (CGO) membrane. Reproduced with permission from ref 106. Copyright 2005 Elsevier.

Using a $scCO_2$ impregnation technique, where the sol–gel precursors were introduced with the aid of SCF into a polymer matrix followed by the sol–gel reactions, polysiloxane/perfluorosulfonic acid membranes were successfully prepared. The resulting materials were characterized for fuel cell applications; the improved performance achieved attributed to a higher proton conductivity and lower methanol permeability.[203]

3.5. Nanocomposites

As well as their hybrid chemical and physical properties, improved thermal and mechanical stabilities were obtained for inorganic–organic nanocomposite materials. For example, a SiO_2/polymer, was synthesized using a range of methods such as blending, sol–gel processing and in situ polymerization.[204,205] Recent interest has focused on in situ sol–gel processing, sol–gel deposition, and a one-pot synthesis of simultaneous sol–gel and polymerization. During the in situ sol–gel process, for instance, small inorganic precursor molecules are transported with SCF molecules that diffuse into the polymer matrix. This takes advantage of the SCF properties including high diffusivity and the ability to effectively swell the polymer phase. The subsequent in situ sol–gel reactions inside the polymer phase ensure an excellent distribution of the inorganic particles within the organic matrix. Using this idea, Han et al and Charpentier et al, respectively, also prepared SiO_2/polypropylene[206] and SiO_2/ polyethylene[178] nanocomposites in $scCO_2$ using TEOS as the precursor. The same approach has been used to prepare TiO_2/activated carbon[207,208] and TiO_2/montmorillonite (MNT) composites,[209–211] where the sol–gel reactions took place inside the pores or layers of the inorganic matrixes with the help of the SCFs.

In the composite materials described in the previous paragraph, metal/silicon oxides are used as fillers incorporated into the matrix of the composite. In another type of composite material, the surfaces of a range of substrates have been decorated with metal oxide nanoparticles using SCFs. Han's group used a variety of metal oxides and deposited them onto carbon nanotubes in SCFs using sol–gel reactions.[112–115,135–137,212,213] For instance, using different mass ratios of $RuCl_3 \cdot 3H_2O$ to carbon nanotubes, RuO_2/carbon nanotube nanocomposites were prepared in supercritical diethyl amine. The TEM images shown in (Figure 19) reveal well-dispersed RuO_2 nanoparticles deposited onto the carbon nanotube surfaces.[137] ZrO_2/carbon nanotubes were prepared from a $Zr(NO_3)_4 \cdot 5H_2O$ precursor and carbon nanotube support in $scCO_2$. The TEM analysis results show (Figure 20) that ZrO_2 formed a layer that covers the exterior surface of the carbon nanotubes, and the thickness of the ZrO_2 layer is a function of the weight ratio of $Zr(NO_3)_4 \cdot 5H_2O$/carbon nanotubes. For comparison, a nanocomposite synthesis was also carried out in ethanol. Results showed that the ZrO_2 formed was mostly isolated from the carbon nanotubes. This suggests that the SCF plays an important role in the ZrO_2 coating on the carbon nanotubes and this is attributed to the zero surface tension of the SCF which enables good wetting of the nanotube surface.[115] Using a similar approach, a thin layer of TiO_2 was also deposited on the molecular sieve SBA-15 in $scCO_2$.[214]

Given the fact that $scCO_2$ is an excellent medium for free radical, cationic and step-growth polymerizations,[38] it is possible to achieve simultaneous sol–gel reactions (for inorganic fillers) and polymerization reactions (for polymer matrix) if the overall reaction rates of the two reaction types are of the same order. Developing on this idea, Charpentier et al prepared SiO_2/poly(vinyl acetate) using a one-pot synthesis in $scCO_2$.[215] In situ ATR-FTIR was used to monitor the decomposition of the polymerization initiator, the consumption of the vinyl acetate monomer and the sol–gel chemistry of the Si precursor. Synchronized sol–gel and polymerization reactions were evident. Both TEM and EDS analysis showed that SiO_2 nanospheres were well-dispersed in the organic polymer matrix.

dx.doi.org/10.1021/cr2000465 | *Chem. Rev.* 2012, 112, 3057–3082

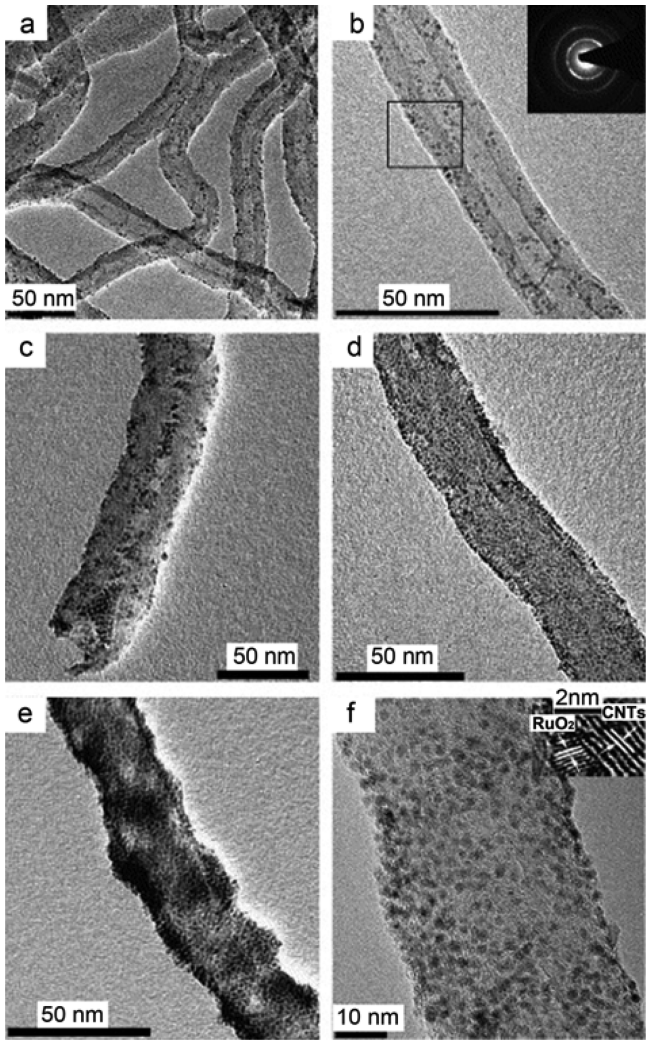

Figure 19. TEM images of the 'as-prepared' composites with different $RuCl_3 \cdot 3H_2O$/carbon nanotube mass ratios: (a, b) 1:2, the inset shows the electron diffraction of the denoted rectangular area; (c) 1:1; (d) 2:1; (e) 3:1; (f and inset) 2:1 high magnification TEM. Reprinted with permission from ref 137. Copyright 2006 Elsevier.

3.6. Solid Templates

Because the morphology and arrangement of the resulting materials can be well controlled, solid templates are extensively used to synthesize well-organized nanostructures. By using a SCF the sol–gel reactants can be transported into the micropores and mesopores of the template, an operation that is difficult using common liquid solvents (Figure 21).[216,217] The

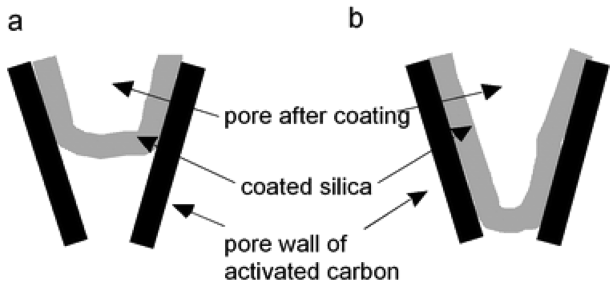

Figure 21. Schematic drawing of SiO_2 coating onto pores of activated carbon in (a) liquid solvent and (b) supercritical solvent, using TEOS as the SiO_2 precursor. Reprinted with permission from ref 217. Copyright 2003 RSC.

subsequent in situ sol–gel reactions occurring inside the templates result in the formation of metal oxides. This is followed by a process to remove the templates, normally a thermal treatment, or by using a reactive plasma or chemical corrosion.[36] One disadvantage of this approach is the cost for template production and removal. The templating method is therefore much more attractive for scale-up when the templates are inexpensive soft materials such as polymers, activated carbon or natural biological materials. All of these are easy to remove afterward through calcination where water and CO_2 are produced.

One example of an inexpensive template is activated carbon which has been used for preparing a number of metal and silicon oxides in $scCO_2$ via sol–gel reactions. For example, Wakayama et al prepared SiO_2 (Figure 22), TiO_2, Al_2O_3 porous fibers with a diameter of a few micrometers using fibrous activated carbon as the templates and metal–organic compounds as the precursors in $scCO_2$.[197,218–222]

Using porous templates that were either synthesized in the laboratory or sourced from natural products, 1-D and mesoporous oxides were prepared via sol–gel reactions in SCFs. Some successfully synthesized examples are: Fe_3O_4 nanowires within the mesopores of SiO_2,[223] TiO_2 nanotubes using collagen fibers of fish[95] as well as cotton fiber templates[196] in $scCO_2$ using either iron dodecarbonyl or TTIP as the precursors. In addition, mesoporous SiO_2, TiO_2, TiO_2/SiO_2 and Al_2O_3/Fe_2O_3 were prepared using block copolymers, activated carbon, starch gel, and bamboo membrane as the templates.[36,224–228]

Using templates of monodispersed polystyrene (PS) latex with different functional groups, Cabanas et al prepared well-defined macroporous SiO_2 aerogels in $scCO_2$ using the hydrolysis and condensation of TMOS and TEOS (Figure 23 a-c).[229–231] A template of 3-D latex arrays was prepared by

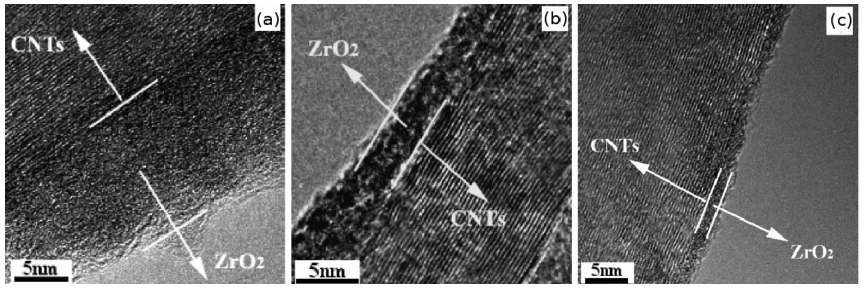

Figure 20. HRTEM images of ZrO_2/carbon nanotubes prepared with different weight ratios of $Zr(NO_3)_4 \cdot 5H_2O$/carbon nanotube: (a) 4:1, (b) 2:1, and (c) 1:1. Reprinted with permission from ref 115. Copyright 2006 American Chemical Society.

dx.doi.org/10.1021/cr2000465 | Chem. Rev. 2012, 112, 3057–3082

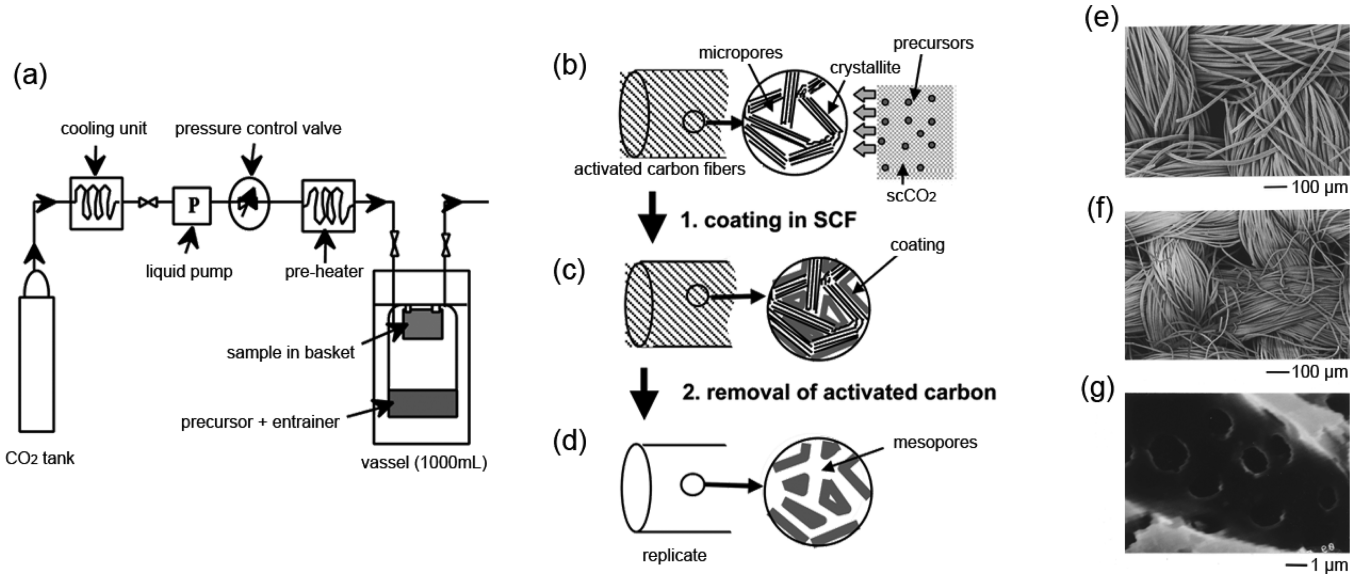

Figure 22. (a) Experimental setup and (b–d) schematic drawing of the casting process using activated carbon fibers as the template. Reproduced with permission from ref 220. Copyright 2006 American Chemical Society. SEM images of (e) activated carbon fibers and (f and g) silica sample calcined in air at 873 K after the treatment in supercritical fluids. Reproduced with permission from ref 218. Copyright 2000 American Chemical Society.

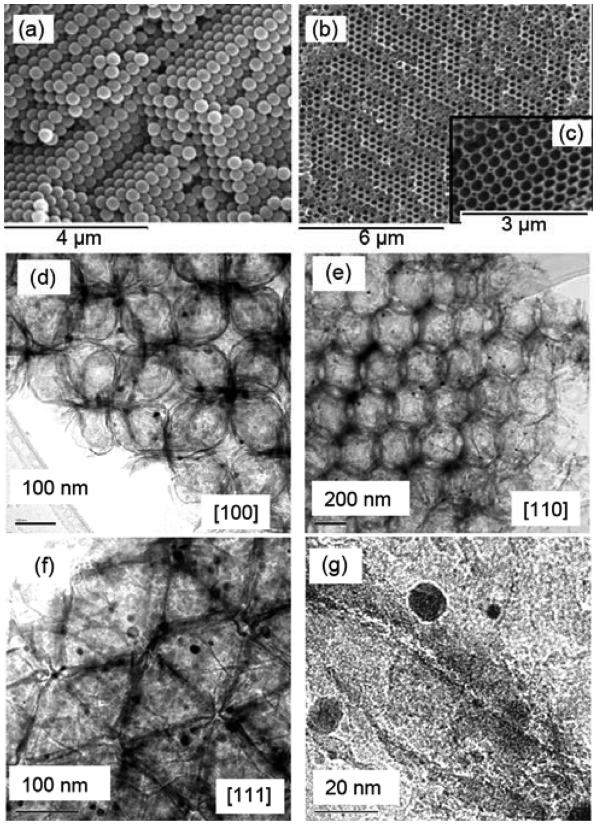

Figure 23. SEM of a latex array template (a) and the periodic macroporous SiO_2 obtained after reaction in $scCO_2$ (b, c). Reproduced with permission from ref 230. Copyright 2005 American Chemical Society. TEM images of an inverse opal obtained by simultaneous reaction and impregnation of TEOS and $Pd(hfa)_2$ in $scCO_2$ into a 3D-latex array template at 303 K and 8.5 MPa and heating in air at 773 K: (d) PdO–SiO_2 and (e–g) Pd–SiO_2 obtained by reduction of the PdO–SiO_2 in H_2/N_2 at 673 K. Reproduced with permission from ref 232. Copyright 2009 Elsevier.

polymerization in a surfactant-free emulsion in water, followed by centrifugation and drying. The sol–gel reactions of TEOS with water were found to take place within the voids of the 3-D template in $scCO_2$, and the resulting materials were calcined at 773 K to remove the polymer template. Recently, PdO-SiO_2 and Pd-SiO_2 aerogel inverse opals were also obtained (Figure 23 d-g) using the approach illustrated in Figure 24.[232] Similarly, SiO_2 and TiO_2 hollow spheres were prepared using cross-linked PS monodispersed microspheres. However, the well-defined template packing pattern was not maintained in the materials produced.[233]

4. THERMODYNAMICS AND KINETICS

To understand the formation of nanostructures in SCFs as described in the above sections, one must consider both the thermodynamic and kinetic factors of the sol–gel chemistry.

4.1. Reaction Equilibrium

From a thermodynamics point of view, the effect of pressure on the reaction equilibrium is determined by the reaction volume ΔV_r, which is defined as the difference between the partial molar volumes of the products and the reactants:[234]

$$\left(\frac{\partial \ln K_x}{\partial p}\right)_{T,x} = -\frac{\Delta V_r}{RT} \tag{19}$$

Here K_x is the mole fraction-based equilibrium constant. According to eq 19, an increase in pressure has a positive effect on the forward reaction when ΔV_r is negative and vice versa. If a product is preferentially transferred into another phase (e.g., the formation of insoluble metal oxides), based on Le Chateliers principle the conversion will increase. For example, in the esterification reaction of acetic acid with ethanol (both of which are used in sol–gel chemistry), the product water has a lower solubility in the $scCO_2$ phase than the two starting materials. Hence, addition of CO_2 to the reaction system drives the forward reaction, and this results in higher conversions.[34,235,236]

dx.doi.org/10.1021/cr2000465 | Chem. Rev. 2012, 112, 3057–3082

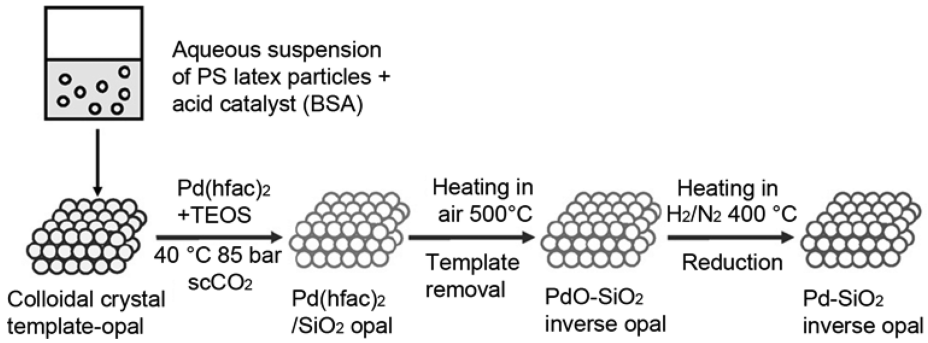

Figure 24. Synthesis of PdO−SiO_2 and Pd−SiO_2 inverse opals in $scCO_2$. Reproduced with permission from ref 232. Copyright 2009 Elsevier.

$$MeCOOH + EtOH \rightleftharpoons MeCO_2Et + H_2O \quad (20)$$

In the case of sol−gel reactions where water is not added to initialize the reaction, the in-situ-generated water resulting from the esterification reaction is quickly consumed in order to hydrolyze the alkoxide precursors (e.g., Si, Ti, and Zr alkoxides).[82,84,87] Metal alkoxides are known to be very active with water and tend to form precipitates when water is added directly. Therefore it is desirable to release water gradually through the esterification reaction and hence to control the consequent sol−gel reactions. This results in well-defined nanostructures. Even though CO_2 is reported to react with TTIP to form complexes in the presence of trace amounts of water,[237] this reaction was not observed using in situ IR during a reaction where TTIP reacted with acetic acid in $scCO_2$.[87,177] This suggests that the reaction with acetic acid is more favorable.

4.2. Solubility

The solubility of a material is one of the most important criteria for an effective sol−gel process. This is because it has an impact on the reaction rate, the yield, the product microstructure as well as the economics of the process.[238] Where the selection of a SCF as a solvent for a sol−gel reaction is concerned, it is a general rule of thumb to choose a higher solubility for the reactants and a lower one for the products. This facilitates the nanostructure formation and downstream separation. It has been found that a higher T_c is favorable for increasing the solubility compared to similar solvents. For example, the supercritical fluids of ethylene (T_c = 282.4 K) and carbon dioxide (T_c = 304.2 K) are better solvents for phenanthrene than nitrogen (T_c = 126.2 K) and methane (T_c = 190.6 K).[239] Generally, a higher pressure increases the solubility of the solute. This behavior is more pronounced near the critical pressure, where the so-called clustering effect increases the solvent density in the adjacent vicinity of the solute molecules compared to the bulk fluid density. The temperature effect is more complicated, because it changes both the density of the SCF and the vapor pressure of the solute. Whereas an elevated temperature increases the solid vapor pressure that promotes the solute solubility, concomitantly it also decreases the SCF density, which has a reverse effect on the solubility.[30]

The solvent power of $scCO_2$ makes it a very attractive medium for the sol−gel reactions of metal alkoxides. This is because of the relatively high solubility of the sol−gel reactants and the reaction intermediates and low solubility of the polycondensate products. Importantly, $scCO_2$ is a good solvent for metal alkoxides that are popular precursors for the sol−gel process (Table 8). In addition, CO_2 molecules are known to interact with carbonyl groups and bridging acetate groups in

Table 8. Solubility of Metal Alkoxides in $scCO_2$ at 313.0 K. Reproduced with Permission from Ref 76. Copyright 1996 PRA Press

metal precursor	solubility (Wt.%)	pressure (MPa)
$Ti(O^iPr)_4$	4.25	8.2
$Ti(OEt)_4$	4.19	12.1
$Ti(O^nBu)_4$	3.05	18.6
$Ti(OCH_2CH(C_2H_5)(CH_2)_2CH_3)_4$	2.21	35.8
$Al(O^iBu)_3$	6.13	>62.0

Lewis-acid and Lewis-base bonding mode, thus the intermediates and colloidal particles with these CO_2-philic moieties can be stabilized in $scCO_2$.[240,241] Another point to note is that the solubility of water in $scCO_2$ is small (most desirable) and this provides a handle for controlling the hydrolysis reaction rate. This is important for the formation of well-defined nanostructures. In addition, the low interaction of water and CO_2 molecules makes the formation of reverse micelles possible when surfactants are added. Hence sol−gel reactions take place within the nanoscale reactors of the micelles, which makes the formation of metal oxide nanoparticles feasible.[78] Finally, the sol−gel products of metal oxides have low solubility in $scCO_2$ which enhances both the separation and the formation of metal oxide particles with uniform dimensions.

Some examples relevant to this review, the solubility of water and acetic acid (polycondensation agents for sol−gel reactions) in CO_2 are shown in Figure 25 a and b, respectively.[242] It should be noted that water has a low solubility, for example, y_2 = 0.0078 at 14 MPa and 333 K. With elevated pressure or temperature, the solubility of the solute increases. This trend is more pronounced for acetic acid in CO_2 with elevated pressure when it gets close to the critical point; indeed, acetic acid and $scCO_2$ are miscible in all proportions at 14 MPa and 333 K.[243] It should also be noted that acetic acid behaves as a cosolvent for the water-CO_2 system. Based on the phase diagram in Figure 26, HOAc and CO_2 are miscible in all proportions at 333 K and 14 MPa; this is also true for the HOAc and H_2O system. On the other hand, CO_2 and H_2O are not miscible in most proportions. However, this can be improved by the addition of HOAc. For example, when HOAc is over ~47 mol % and the mixing rule of Panagiotopoulos and Reid is applied, there is only one phase in the ternary system.[243,244]

The solubility of Cu, Ba, and Y acetylacetonate (acac) and hexafluoroacetylacetonate (hfa) complexes in $scCO_2$ has been measured by Pommier et al.[245] It was found that (1) the solubility of the metal complexes increased with elevated pressure and slightly decreased with lowered temperature and (2) the fluorine-substituted metal carboxylate complexes

dx.doi.org/10.1021/cr2000465 | Chem. Rev. 2012, 112, 3057−3082

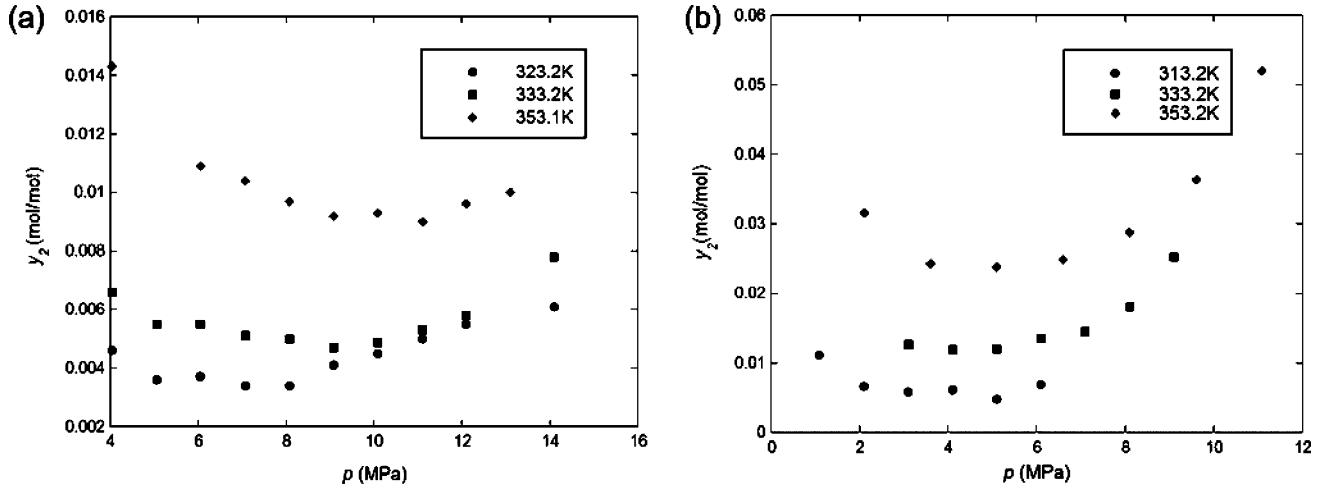

Figure 25. Experimental results for the solubility of water (a) and acetic acid (b) in CO_2. (a) The solubility of water (y_2) increases with elevated pressures (temperature) at a constant temperature (pressure). (b) The solubility of acetic acid increases quickly with elevated pressures when it is close to P_c. Reproduced with permission from ref 242. Copyright 2000 Elsevier.

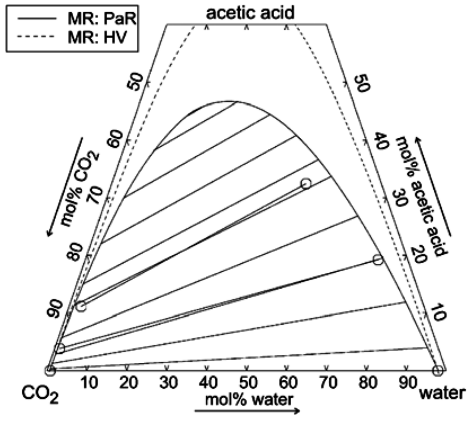

Figure 26. Phase equilibrium of the ternary system CO_2 + H_2O + HOAc at 333 K and 14 MPa. The data points (○) were obtained from experimental measurements, and the predictions from the Peng–Robinson EOS applying the mixing rules of Panagiotopoulos and Reid (PaR) and Huron and Vidal (HV), respectively. Reprinted with permission from ref 243. Copyright 2004 Elsevier.

exhibited a significantly higher solubility than the non-substituted complexes. Additional solubility data of metal complexes in $scCO_2$ has been summarized by Darr and Poliakoff.[39]

Metal oxides are known for their low solubility in most solvents. However, the oxides can exhibit enhanced dissolving capacity in SCFs,[246] which has an effect on the stability of the colloidal particulates and their nucleation rate during the sol–gel process. While a very low solubility of metal oxides in conventional solvents under ambient pressure results in a supersaturated solution and consequently quick precipitation, a moderate solubility will facilitate a progressive nucleation (gelation) process during the sol–gel reactions. Therefore, it is by no means a trivial matter to study the solubility of metal oxides in SCFs and to seek out the best conditions (e.g., temperature and pressure) for the process. Even though there is a significant lack of solubility data of oxides available for the SCF process, previous experimental results show a moderate solubility in SCW.[247] The solubility of SiO_2 in subcritical and supercritical H_2O has been studied for the temperature range 437–873 K and the pressure range 15.2–177.3 MPa. From Figure 27 it can be observed that a higher pressure enhances the solubility of quartz in SCW, whereas the temperature has a

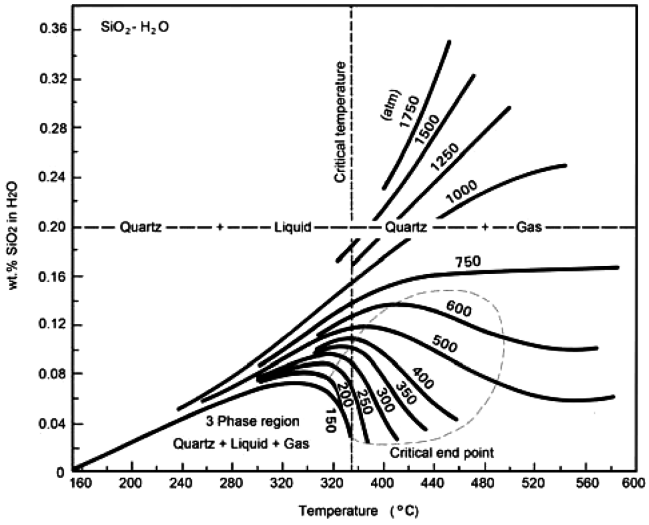

Figure 27. Solubility of SiO_2 (quartz form) in subcritical and supercritical H_2O. The area enclosed by the dashed line is the region of retrograde solubility. Reprinted with permission from ref 246. Copyright 1989 Wiley.

more complex effect on the solubility. It is positive above a pressure of 101.3 MPa (1000 atm) and it is mostly negative below a pressure 60.8 MPa (600 atm).[248] It should also be noted that the solubility of metal oxides in SCW are a function of pH, for example, a higher pH promoted the solubility of TiO_2 in the temperature range 370–600 K and 30 MPa.[139]

A stringent thermodynamic calculation can be carried out using an equation of state (EOS), for example, the Redlich–Kwong equation and the Peng–Robinson equation,[75,238,249,250] for many small molecules with known thermodynamic properties, such as critical points, acentric factors and interaction parameters. For macromolecules and other more complex compounds, group contribution and solubility parameter approaches are more practical for predicting the solubility semiquantitatively.[251–254] Using these empirical equations, for example, the solubility parameters of the

dx.doi.org/10.1021/cr2000465 | Chem. Rev. 2012, 112, 3057–3082

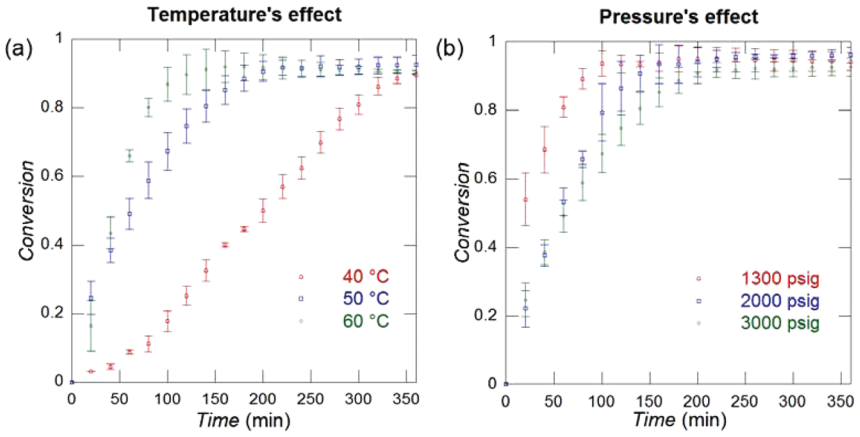

Figure 28. (a) Temperatures and (b) pressures effect on the precursor conversion of TEOS within a reaction time of 0−360 min. In a, the source IR data was obtained at a constant pressure of 3000 psig (20.68 MPa); in b, the source IR data was obtained at a constant temperature of 327.2 K; the initial concentrations of TEOS and HOAc was 0.088 and 0.362 M, respectively. Reprinted with permission from ref 177. Copyright 2008 American Chemical Society.

macromolecules of $[Ti_6O_9(C_2H_3O_2)_6]_n$ and $[Ti_4Zr_2O_7(C_2H_3O_2)_{10}(^iC_3H_7O)_2]_n$ were estimated by Charpentier et al.[255]

It is important to point out within the context of this review that understanding the solubility during sol−gel reactions in a SCF is in fact rather complicated: sol and gel of metal complexes (or oxides) appear in the SCF in the polycondensation process with ever changing concentrations of cosolvents, for example, ethanol, ester and H_2O that are intermediates or byproduct of the reactions. The presence of these cosolvents also changes the properties of the reaction media such as the polarity, the critical points, phase equilibrium, as well as the number of phases.[256]

4.3. Reaction Kinetics in Supercritical Fluids

A noteworthy limitation of the conventional sol−gel synthetic process using organic solvents is related to the sol−gel reaction kinetics. Some sol−gel reactions are either too slow for commercialization or too fast for effective process control under ambient synthesis conditions. For example, when metal nitrates (which are cheaper than metal alkoxides) are used as the sol−gel precursors for preparing metal oxide nanoparticles, the overall reaction rate is very slow in the conventional aqueous sol−gel process. In this case a SCF process becomes attractive, not only because of the higher mass and heat transfer in the SCF facilitating the reactions, but also because the reaction kinetics can be tuned by changing the reaction temperature and pressure. In supercritical organic solvents or supercritical water, for instance, a desirable reaction rate can be achieved with a higher temperature, well above the boiling point of the solvent.[257,258] Another example is the hydrolysis and condensation rates of some metal alkoxides (e.g., titanium, zirconium and aluminum alkoxides) which are so rapid that it is difficult to control the size and shape of the resulting materials. Therefore, an aqueous solution is not suitable for these types of sol−gel reactions. This problem is circumvented by using nonaqueous sol−gel reactions where the reaction kinetics are better controlled, thus facilitating the formation of well-defined nanostructures.[66,119,259]

Unlike the conventional sol−gel process, the reaction kinetics of sol−gel reactions in SCFs are a function of pressure in addition to reaction temperature and reactant concentrations. For instance, the conversion of TEOS was studied as a function of temperature and pressure in $scCO_2$ using in situ FTIR and a chemometrics modeling technique (Figure 28).[177] From Figure 28 it can be observed that a higher temperature and low pressure facilitate the conversion in the region of 313−333 K and 1300−3000 psig (8.96−20.68 MPa), respectively. The effect of the temperature on the kinetics is consistent with the Arrhenius equation. The pressure effect may be explained by the significant clustering effect at the supercritical point, given the fact that 1300 psi (8.96 MPa) is close to the P_c of CO_2 (7.375 MPa) in the presence of acetic acid. A higher local concentration of acetic acid with TEOS will increase the reaction rate. In another example, Pommier et al followed the conversion of TTIP using offline FTIR measurements during their synthesis of TiO_2 in supercritical isopropanol. The overall reaction was found to follow first-order kinetics, and 113 kJ/mol was the apparent activation energy obtained.[122]

5. REACTOR DESIGN AND IN SITU ANALYSIS

The chemical reactor is the most important component of the reaction system, hence a number of reactors are available for sol−gel reactions in SCFs on a laboratory scale: a conventional cylinder-shape autoclave with an agitator and heating system, a view cell with sapphire windows, a T-shape, or a coaxial nozzle reactor for mixing of fluid streams. Depending on the reaction temperature and type of chemicals involved, different types of materials have been used for the reactor construction, for example, 316 stainless steel for $scCO_2$ and supercritical alcohols, and Hastelloy lined metal autoclaves for SCW, which suffers from serious corrosion issues.

5.1. Batch Reactors

A batch reactor is generally used to prepare monolithic and particulate aerogels with a wide range of morphologies as described earlier in this review. Autoclaves or view cell reactors are used to prepare SiO_2, TiO_2, ZrO_2, and ZrO_2−TiO_2 monoliths.[80,81,83,84] For instance, when equipped with sapphire windows, the view cell (10−25 mL) is ideal for observing the phase change, particle formation, and small-scale material synthesis in SCFs (Figure 29).[83] This view cell system can be used for the preparation of a few grams of metal oxides, while an autoclave with agitator and large interior volume (e.g., 500 mL) is better for large-scale production (tens to hundred grams).

dx.doi.org/10.1021/cr2000465 | Chem. Rev. 2012, 112, 3057−3082

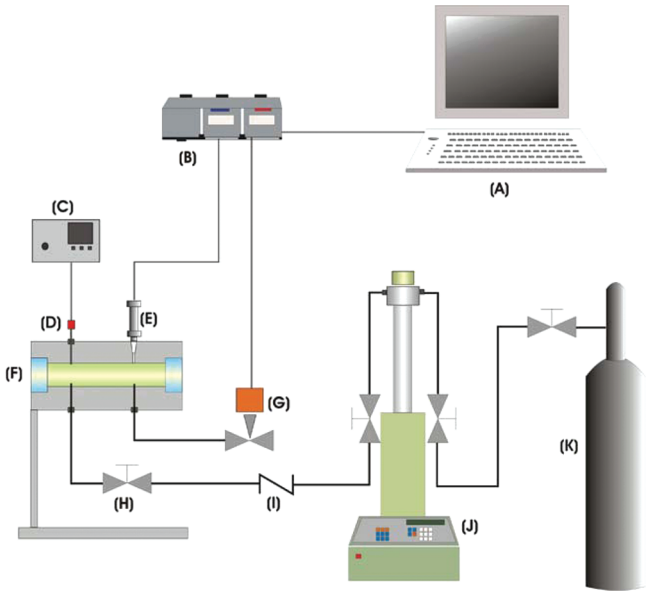

Figure 29. Schematic of a batch reactor for $scCO_2$: (A) computer with Labview Virtual Instrument, (B) FieldPoint by National Instrument, (C) temperature controller, (D) thermocouple, (E) pressure transducer, (F) stainless steel view cell equipped with sapphire windows (in blue), (G) pneumatic valve controlled by the computer, (H) needle valve, (I) check valve, (J) syringe pump, and (K) CO_2 cylinder. Reprinted with permission from ref 83. Copyright 2005 American Chemical Society.

5.2. Continuous Reactors

Continuous reactors are suitable for producing particulates when sol–gel reactions are rapid. For example, Reverchon et al designed a continuous reactor for producing TiO_2 submicrometer particles (Figure 30), taking advantage of the fast reaction rate of Ti alkoxides with water.[92] In this reaction system, liquid CO_2 from the reservoir (V1) was pumped through a drying vessel (D) filled with dry SiO_2 gel and a heat exchanger, before it dissolved the sol–gel precursor in the contact vessel (V2). At the same time, CO_2 was pumped into another contactor (V3) where water was added. In the reactor (R), the precursor–SCF solution contacts the H_2O-SCF stream at the coaxial injection system, which allowed a quick sol–gel reaction and formation of metal oxide particles. Then CO_2 was recycled through a micrometering valve (VM) and a liquid separator (LS).[92]

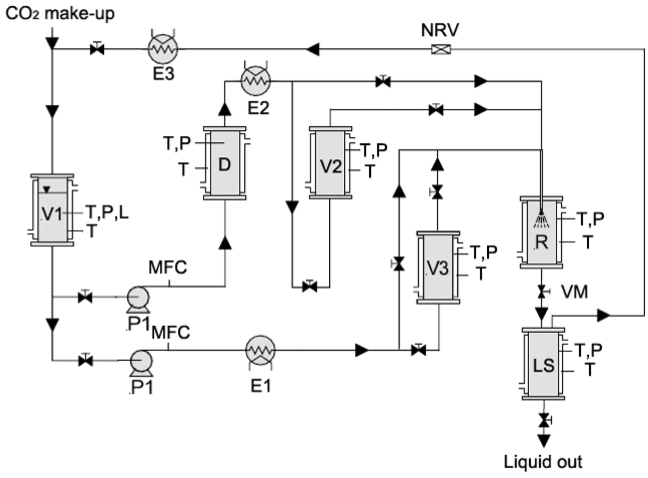

Figure 30. Schematic of the continuous pilot plant for production of TiO_2 particles: V1, CO_2 storage vessel; V2, CO_2–TTIP contactor; V3, CO_2–H_2O contactor; D, CO_2 dryer; R, reaction vessel; LS, liquid separator; MFC, mass flow control; NRV, nonreturn valve; VM, micrometering valve. Reproduced with permission from ref 92. Copyright 2003 Elsevier.

A T-shape reactor, where two streams meet one another, has been widely used to produce metal oxide nanoparticles in a continuous manner. One of the disadvantages of the T-shape continuous reactor, however, is that the particles tend to accumulate in the reactor after a certain period of time. This causes variations in contact time and consequently a wide particle size distribution. In order to improve the reliability of the SCW process for producing metal oxide nanoparticles, Paliakoff et al designed a nozzle reactor (Figure 31) based on light adsorption imaging and computational fluid dynamics modeling.[141] To form smaller particles with a narrow particle-size distribution and to prevent premature precipitation and particle accumulation, the criteria of the SCW reactor includes: (1) instantaneous and homogeneous mixing of the SCW with metal salt streams, (2) short average residence time, (3) minimal heating of the aqueous metal salt stream prior to the reactor, and (4) rapid transport of product particles out of the reactor.[141]

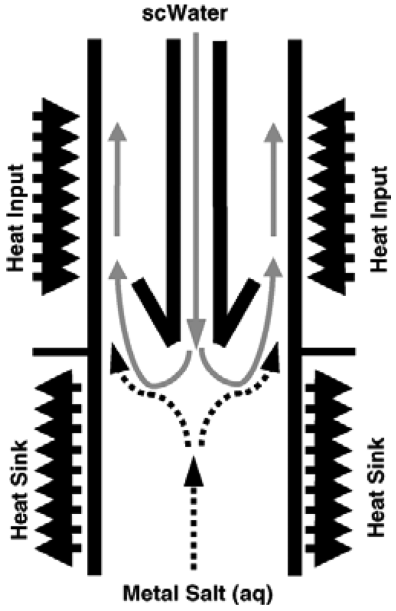

Figure 31. Schematic of the nozzle reactor design with ideal heating/cooling profile. The SCW is fed downward through the internal pipe while the aqueous salt stream is fed counter-currently upward through the outer pipe. The product particles are formed and immediately transported out of the hot-zone of the reactor. Reprinted with permission from ref 141. Copyright 2006 Elsevier.

5.3. In Situ Analysis Techniques

To study the reaction mechanism, thermodynamics and kinetic processes of the sol–gel reactions along with potential industrial online analysis, it is necessary to analyze the chemical compositions in the fluid phase. For instance, immediate GC-MS and NMR analysis was carried out to study the intermediate chemical structures during reactions of TMOS with acetic acid in $scCO_2$.[178] Results demonstrated the

dx.doi.org/10.1021/cr2000465 | Chem. Rev. 2012, 112, 3057–3082

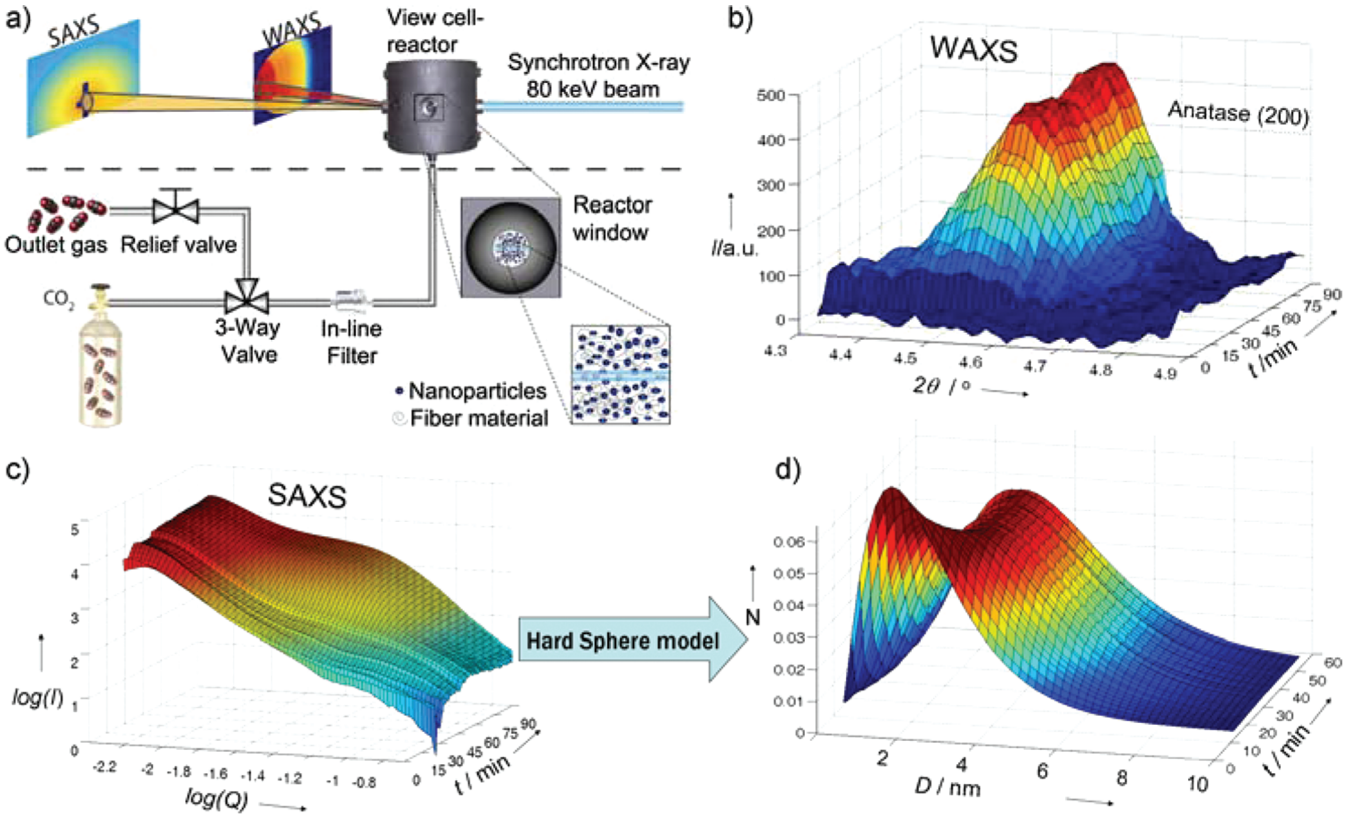

Figure 32. Experimental setup for real-time, in situ SAXS/WAXS studies of supercritical reactions (a). The development of crystallinity can be monitored by WAXS, as exemplified by the anatase (200) reflection (b). The SAXS data (c) provide information on mesostructure, and particle size distribution (diameter) was extracted by using a hard-sphere model (d). Reprinted with permission from ref 93. Copyright 2007 Wiley InterScience Publishers.

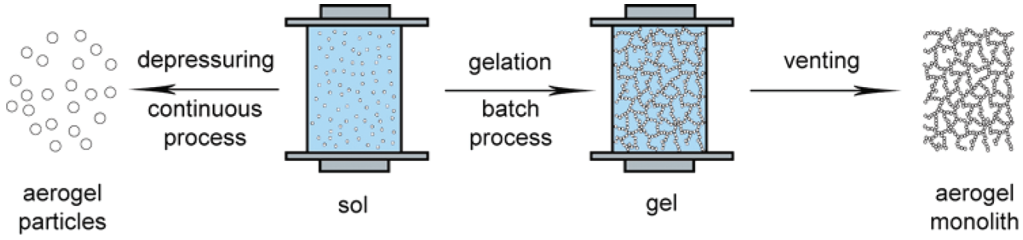

Figure 33. Schematic formation of aerogel particles and monolith using sol–gel reactions in SCF.

existence of the bridging $-OCH_3$ group for the first time thus facilitating an understanding of the reaction mechanism. However, often it is not convenient to take a sample for immediate offline analysis where sol–gel reactions in SCFs is concerned. This is because the rapidly formed particles tend to block the sampling tubes and valves upon the pressure drop, and the release of the SCF might result in a significant pressure drop for a benchtop scale autoclave. Thus in situ analysis techniques are more convenient for monitoring the reaction system because they can be carried out with no disturbance of the reactions.

To date, in situ analysis techniques for studying sol–gel reactions in SCFs include ATR-FTIR and high-energy synchrotron radiation. ATR-FTIR equipment with a high-pressure probe is indispensable for monitoring such chemical reactions in high-pressure vessels. For instance, the sol–gel reaction mechanism[87] and kinetics[177,260] in $scCO_2$, as well as solvent effects[240,261] have been studied using in situ IR techniques with several of the published results described above. For example, an ATR-IR cell was used to study the intermolecular interaction of CO_2 and PMMA, where the polymer was deposited onto the surface of ZnSe crystal to minimize the absorbance from bulk CO_2.[241]

Despite its rarity and lack of availability, a high-energy (80 keV) synchrotron technique provides real-time, in situ information for simultaneous small-angle X-ray scattering (SAXS) and wide-angle X-ray scattering (WAXS). This combination provides information on both the particle size and crystallization processes. This technique has also been used for monitoring the formation of TiO_2 nanocrystallites in $scCO_2$ via the sol–gel route.[93] Figure 32 shows the experimental setup for the in situ synchrotron radiation techniques for monitoring a view cell reactor, the scanned 3-D WAXS and SAXS spectra, and the calculated particle size distribution from the SAXS data. In order to decrease the cost for such in situ X-ray studies, a new experimental setup was developed by Iversen et al.[262] Here by using a lower photon energy of 11.2 keV and sapphire

dx.doi.org/10.1021/cr2000465 | Chem. Rev. 2012, 112, 3057–3082

capillary batch reactor, formation of ZrO_2 in SCW was able to be studied by in situ SAXS/WAXS.

6. SUMMARY AND OUTLOOK

Although both the individual sol−gel and SCF drying steps are established protocols for preparing porous nanomaterials, the direct sol−gel reaction in SCFs is a relatively new synthetic technique. As described throughout this review, by using this technique a variety of metal oxides with 0-D (nanospheres), 1-D (nanofibers), 2-D (membrane), and 3-D (monolith) morphologies have been successfully prepared. The sol−gel precursors are often selected because of their ability to dissolve in the SCF, for example, metal acetate and alkoxides in supercritical organic solvents, metal nitrates and acetates in SCW, and alkoxides and acetates in $scCO_2$. In a high-pressure vessel, the sol−gel precursors are transformed into sols through polycondensation reactions in the SCF, and these sols can be either depressurized to form aerogel particles (often in a continuous reactor) or used for building blocks of gel solid networks (in a batch reactor). This is illustrated schematically in Figure 33. The aerogel particles normally have larger dimensions than the sols due to the coalescence and aggregation steps. Whereas the aerogel monolith maintains the size and shape of the original gel; unlike the xerogel that shrinks upon evaporative drying.

High-temperature SCF techniques, that is, supercritical water and organic solvents, have been successfully utilized for synthesizing metal oxide particles. This technique is attractive for potential commercialization because the reactions are rapid, which facilitates a potentially continuous process. The resulting materials are also readily crystalline, which saves a separate calcination unit operation. One promising potential application of the continuous SCF reactor might be a one-step synthesis of monodispersed nanoparticles of mixed metal oxides, which often show better physiochemical properties for their applications as catalysts and semiconductors than the single component metal oxide. These emerging materials have tremendous advantages in the next generation of photocatalytic reactors, as well as in alternative energy processes, including photovoltaics and catalysts for gasification. Depending on the reactor design, the multicomponent metal oxides can exhibit either homogeneous distribution or spatially separated including core−shell structure.

In terms of low-temperature SCF techniques (i.e., $scCO_2$), direct sol−gel methods have been developed for preparing both particulates and monoliths of metal oxide aerogels. Depending on the reaction kinetics, the process can either allow continuous production of particles or batch preparation of monoliths. The state of art achievement in this field is manipulating the nanostructures of metal oxides using self-assembly of metal complexes through favorable chemistry or using soft templates (e.g., surfactants, polymer and organic materials). The control of nanostructure growth is essential for the fabrication of nanosemiconductor devices using the scalable $scCO_2$ process.[263] To prepare electrodes for dye-sensitized solar cells, for example, TiO_2 nanowire arrays can be manipulated to grow from functionalized conductive glass[264] using linear polycondensation chemistry in $scCO_2$. The high surface area and the delicate nanowire arrays of TiO_2 can be maintained after CO_2 venting, hence efficient energy conversion is promoted.[265] Besides the strategy of using the controlled polycondensation of metal complexes, the design of sol−gel derived nanostructures in $scCO_2$ could be accomplished by using capping ligands that selectively quench crystal growth in certain directions.[40] The same goal might be achieved by using other methodologies in a supercritical medium such as supercritical fluid transport-chemical deposition of film (SFT-CD),[266] supramolecular assemblies and 1-D material formation using organogelators.[267] These techniques take advantage of the better mass and heat transfer properties available in SCFs compared to their counterpart gas or liquid phase reactions.

Another potential field ready to explore is the synthesis of inert metal oxide cages with biological catalysts (e.g., enzymes) trapped within using $scCO_2$. The advantages of this technique are 2-fold. First, the high porosity of the areogels provides a "basket" for entrapment of the enzyme that is accessible to the reactants and at the same time facilitates the downstream separation process.[268] Second, the mild temperatures accessible in $scCO_2$ ensures that the enzymes will survive the sol−gel reactions, unlike the hydrothermal process for synthesizing zeolites that will only kill the organisms. This type of catalyst is of interest for wastewater treatment and H_2S removal for natural gas industries among other applications.

In order to be able to control the morphology of these nanomaterials for next generation applications in alternative energy and biotechnology, the mechanism of formation will need to be better understood. In situ studies are required using advanced analytical tools. Several high pressure analysis techniques, for example, TRIR,[269,270] UV, NMR,[271−273] EPR, and Raman,[274] have all been used for various studies on the interactions of SCF and solutes and monitoring chemical reactions in SCFs.[30] However, these in situ techniques have not yet been documented for studying direct sol−gel process in SCFs. Such investigations will provide a more detailed understanding of reaction mechanisms which in turn will allow morphology control and controlled chemistries for integration into polymers or attachments to surfaces for next generation materials and devices. It is hoped that this review will contribute to a greater understanding of the current state of research in this exciting and emerging field as well as stimulate future research.

AUTHOR INFORMATION

Corresponding Author

*E-mail: pcharpentier@eng.uwo.ca. Phone: 1-519-661-3466. Fax: 1-519-661-3498.

Biographies

dx.doi.org/10.1021/cr2000465 | Chem. Rev. 2012, 112, 3057−3082

Ruohong Sui received his B.S. degree in chemistry from Heilongjiang University and his Ph.D. in chemical engineering at University of Western Ontario, under the direction of professors Paul A. Charpentier and Amin S. Rizkalla. During graduate school, he synthesized TiO_2, ZrO_2, and SiO_2 materials with a variety of nanoarchitectures in supercritical CO_2. After graduate studies, he joined Curtis P. Berlinguette's group at the University of Calgary and worked on synthesizing semiconducting nanowire arrays on conductive glass for solar cell applications. He is currently a Natural Science and Engineering Research Council's (NSERC) industrial R&D fellow at Alberta Sulphur Research Ltd, under the supervision of Peter D. Clark. His projects include synthesizing hybrid metal oxide nanomaterials for SO_2 separation and new catalysts for CO oxidation, and developing a new Claus tail gas process for oil and natural gas industries.

Paul A. Charpentier is a Professor of Chemical & Biochemical Engineering at the University of Western Ontario. He received M. Sc. From the University of Waterloo and Ph. D. at McMaster University. Dr. Charpentier's research focuses on developing "green nanotechnologies" using supercritical fluids to prepare well-defined nanostructures, such as metal oxides and polymer nanocomposites for their applications in the areas of catalysis and alternative energy conversion. His current projects include using supercritical carbon dioxide as working media for preparing one-dimensional metal oxides with a high surface area, and the resulting semiconductor nanofiber or nanotube arrays will be incorporated into the thin-film dye-sensitized solar cells for low-cost and high-yield sunlight harvest. Recent awards include the Ontario Premier's Research Excellence Award (2002), Petro-Canada Young Innovator Award (2007), Western Faculty Scholar Award (2010) and Western Innovator Award (2010).

ACKNOWLEDGMENTS

This work was financially supported by the Canadian Natural Science and Engineering Research Council (NSERC), the Materials and Manufacturing Ontario Emerging Materials program (MMO-EMK), the Canadian Foundation for Innovation (CFI), and the UWO Academic Development Fund (ADF).

ABBREVIATIONS

acac	acetylacetonate
am	amorphous
ASOG	analytical solutions of group
ATR-FTIR	attenuate total reflection-Fourier transform infrared spectrometry
BSA	benzosulfonic acid
CVD	chemical vapor deposition
cont	continuous
CTAB	cetyltrimethyl-ammonium bromide
DSC	differential scanning calorimetry
DSSC	dye-sensitized solar cell
EDS	energy dispersive X-ray spectroscopy
EOS	equation of state
EPR	electron paramagnetic resonance
ESI-MS	electrospray ionization mass spectrometry
hfa (or hfac)	hexafluoroacetylacetonate
HOAc	acetic acid
HRTEM	high resolution transmission electron microscopy
HTS-SCW	hydrothermal synthesis in supercritical water
MNT	Na-Montmorillonite
OAc	acetate
P_c	critical pressure
PEO-PPO-PEO	poly(ethylene oxide)-*b*-poly(propylene oxide)-*b*-poly(ethylene oxide)
PMMA	poly(methyl methacrylate)
PS	polystyrene
SAXS	small-angle X-ray scattering
$scCO_2$	supercritical CO_2
SCF	supercritical fluid
SCW	supercritical water
SEM	scanning electron microscopy
T_c	critical temperature
TEM	transmission electron microscopy
TEOS	tetramethyl orthosilicate
TGA	thermogravimetric analysis
TMOS	tetraethyl orthosilicate
TRIR	time-resolved infrared spectroscopy
TTBO	titanium tetrabutoxide
TTIP	titanium tetraisopropoxide
VLE	vapor−liquid equilibrium
VOCs	volatile organic compounds
WAXS	wide-angle X-ray scattering
ZSM	Mn-doped zinc silicate

REFERENCES

(1) Nagaveni, K.; Sivalingam, G.; Hegde, M. S.; Madras, G. *Appl. Catal., B* **2004**, *48*, 83.
(2) Fernandez-Garcia, M.; Martinez-Arias, A.; Hanson, J. C.; Rodriguez, J. A. *Chem. Rev.* **2004**, *104*, 4063.
(3) Gratzel, M. *Inorg. Chem.* **2005**, *44*, 6841.
(4) Archanjo, B. S.; Silveira, G. V.; Goncalves, A.-M. B.; Alves, D. C. B.; Ferlauto, A. S.; Lacerda, R. G.; Neves, B. R. A. *Langmuir* **2008**, *25*, 602.
(5) Harnack, O.; Pacholski, C.; Weller, H.; Yasuda, A.; Wessels, J. M. *Nano Lett.* **2003**, *3*, 1097.
(6) Long, J. W.; Dunn, B.; Rolison, D. R.; White, H. S. *Chem. Rev.* **2004**, *104*, 4463.
(7) van den Bossche, M.; McIntosh, S. *Chem. Mater.* **2010**, *22*, 5856.
(8) Bartholomew, C. H.; Farrauto, R. J. *Fundamentals of Industrial Catalytic Processes*; Wiley-Interscience, 2006.
(9) Pajonk, G. M. *Appl. Catal.* **1991**, *72*, 217.
(10) Law, M.; Greene, L. E.; Johnson, J. C.; Saykally, R.; Yang, P. *Nat. Mater.* **2005**, *4*, 455.
(11) Shankar, K.; Bandara, J.; Paulose, M.; Wietasch, H.; Varghese, O. K.; Mor, G. K.; LaTempa, T. J.; Thelakkat, M.; Grimes, C. A. *Nano Lett.* **2008**, *8*, 1654.
(12) Zaera, F. *J. Mater. Chem.* **2008**, *18*, 3521.
(13) Shen, G.; Chen, P.-C.; Ryu, K.; Zhou, C. *J. Mater. Chem.* **2009**, *19*, 828.

(14) Ziegler, K.; Ryan, K. M.; Rice, R.; Crowley, T.; Erts, D.; Olin, H.; Patterson, J.; Spalding, T. R.; Holmes, J. D.; Morris, M. A. *Faraday Discuss.* **2004**, *125*, 311.
(15) Gurlo, A.; Barsan, N.; Wemar, U. In *Metal Oxides: Chemistry and Applications*; Fierro, J. L. G., Ed.; CRC Press: Boca Raton, FL, U.S.A., 2006.
(16) Oliveira, A. P. A; Hochepied, J.-F.; Grillon, F.; Berger, M.-H. *Chem. Mater.* **2003**, *15*, 3202.
(17) Okuyama, K.; Kousaka, Y.; Tohge, N.; Yamamoto, S.; Wu, J. J.; Flagan, R. C.; Seinfeld, J. H. *AIChE J.* **1986**, *32*, 2010.
(18) Chang, P.-C.; Fan, Z.; Wang, D.; Tseng, W.-Y.; Chiou, W.-A.; Hong, J.; Lu, J. G. *Chem. Mater.* **2004**, *16*, 5133.
(19) Liu, S. M.; Gan, L. M.; Liu, L. H.; Zhang, W. D.; Zeng, H. C. *Chem. Mater.* **2002**, *14*, 1391.
(20) Therese, G. H. A.; Kamath, P. V. *Chem. Mater.* **2000**, *12*, 1195.
(21) Li, D.; Xia, Y. *Nano Lett.* **2003**, *3*, 555.
(22) Adschiri, T.; Hakuta, Y.; Arai, K. *Ind. Eng. Chem. Res.* **2000**, *39*, 4901.
(23) Li, T.; Moon, J.; Morrone, A. A.; Mecholsky, J. J.; Talham, D. R.; Adair, J. H. *Langmuir* **1999**, *15*, 4328.
(24) Hench, L. L.; West, J. K. *Chem. Rev.* **1990**, *90*, 33.
(25) West, R. H.; Beran, G. J. O.; Green, W. H.; Kraft, M. *J. Phys. Chem. A* **2007**, *111*, 3560.
(26) Schmidt, H.; Jonschker, G.; Goedicke, S.; Mennig, M. In *Sol–Gel Science and Technology*; Sakka, S., Ed.; Springer, 2002; Vol. *3*.
(27) Bradley, D. C. *Alkoxo and Aryloxo Derivatives of Metals*; Academic Press: San Diego, CA, U.S.A, 2001.
(28) Roy, R. *Science* **1987**, *238*, 1664.
(29) Baccile, N.; Babonneau, F.; Thomas, B.; Coradin, T. *J. Mater. Chem.* **2009**, *19*, 8537.
(30) Leitner, W.; Jessop, P. G. *Chemical Synthesis Using Supercritical Fluids*; Wiley-VCH: Weinheim, Germany, 1999.
(31) Giddings, J. C.; Myers, M. N.; McLaren, L.; Keller, R. A. *Science* **1968**, *162*, 67.
(32) Kajimoto, O. *Chem. Rev.* **1999**, *99*, 355.
(33) Johnston, K. P.; Haynes, C. *AIChE J.* **1987**, *33*, 2017.
(34) Blanchard, L. A.; Brennecke, J. F. *Green Chem.* **2001**, *3*, 17.
(35) Johnston, K. P.; Shah, P. S. *Science* **2004**, *303*, 482.
(36) Pai, R. A.; Humayun, R.; Schulberg, M. T.; Sengupta, A.; Sun, J.-N.; Watkins, J. J. *Science* **2004**, *303*, 507.
(37) Fenghour, A.; Wakeham, W. A.; Vesovic, V. *J. Phys. Chem. Ref. Data* **1998**, *27*, 31.
(38) Kendall, J. L.; Canelas, D. A.; Young, J. L.; DeSimone, J. M. *Chem. Rev.* **1999**, *99*, 543.
(39) Darr, J. A.; Poliakoff, M. *Chem. Rev.* **1999**, *99*, 495.
(40) Shah, P. S.; Hanrath, T.; Johnston, K. P.; Korgel, B. A. *J. Phys. Chem. B* **2004**, *108*, 9574.
(41) Aymonier, C.; Loppinet-Serani, A.; Reverón, H.; Garrabos, Y.; Cansell, F. *J. Supercrit. Fluids* **2006**, *38*, 242.
(42) Bahrami, M.; Ranjbarian, S. *J. Supercrit. Fluids* **2007**, *40*, 263.
(43) Reverchon, E.; Adami, R. *J. Supercrit. Fluids* **2006**, *37*, 1.
(44) Reverchon, E.; Adami, R.; Caputo, G.; De Marco, I. *J. Supercrit. Fluids* **2008**, *47*, 70.
(45) Beckman, E. J. *J. Supercrit. Fluids* **2004**, *28*, 121.
(46) Seki, T.; Baiker, A. *Chem. Rev.* **2009**, *109*, 2409.
(47) Bellet, D.; Canham, L. *Adv. Mater.* **1998**, *10*, 487.
(48) Scherer, G. W. *J. Am. Ceram. Soc.* **1990**, *73*, 3.
(49) Bisson, A.; Rigacci, A.; Lecomte, D.; Rodier, E.; Achard, P. *Drying Technol.* **2003**, *21*, 593.
(50) Gogotsi, Y.; Libera, J. A.; GuÄvencÂ-Yazicioglu, A.; Megaridis, C. M. *Appl. Phys. Lett.* **2001**, 79.
(51) Kistler, S. S. *J. Phys. Chem.* **1932**, *36*, 52.
(52) Dutoit, D. C. M.; Schneider, M.; Baiker, A. *J. Catal.* **1995**, *153*, 165.
(53) Lam, U. T.; Mammucari, R.; Suzuki, K.; Foster, N. R. *Ind. Eng. Chem. Res.* **2008**, *47*, 599.
(54) Pierre, A. C.; Pajonk, G. M. *Chem. Rev.* **2002**, *102*, 4243.
(55) Fricke, J.; Emmerling, A. *J. Sol–Gel Sci. Technol.* **1998**, *13*, 299.
(56) Brinker, C. J.; Scherer, G. W. *Sol–Gel Science: The Physics and Chemistry of Sol–Gel Processing*; Academic Press: New York, 1990.
(57) Scherer, G. W. *J. Sol–Gel Sci. Technol.* **1994**, *3*, 127.
(58) Scherer, G. W. *J. Non-Cryst. Solids* **1992**, *145*, 33.
(59) Matejová, L.; Cajthaml, T.; Matej, Z.; Benada, O.; Kluson, P.; Solcová, O. *J. Supercrit. Fluids* **2010**, *52*, 215.
(60) Liong, K. K.; Wells, P. A.; Foster, N. R. *J. Supercrit. Fluids* **1991**, *4*, 91.
(61) Unlusu, B.; Sunol, A. K. *Fluid Phase Equilib.* **2004**, *226*, 15.
(62) Ebelmen. *Aether Ann. Chim. Phys.* **1846**, No. Series 3, 319.
(63) Gesser, H. D.; Goswami, P. C. *Chem. Rev.* **1989**, *89*, 765.
(64) Hüsing, N.; Schubert, U. *Angew. Chem., Int. Ed.* **1998**, *37*, 22.
(65) Pierre, A. C. *Introduction to Sol–Gel Processing*; Kluwer Academic Publishers: Boston, MA, U.S.A., 1998.
(66) Niederberger, M. *Acc. Chem. Res.* **2007**, *40*, 793.
(67) Niederberger, M.; Garnweitner, G. *Chem.—Eur. J.* **2006**, *12*, 7282.
(68) Niederberger, M.; Garnweitner, G.; Buha, J.; Polleux, J.; Ba, J.; Pinna, N. *J. Sol–Gel Sci. Technol.* **2006**, *40*, 259.
(69) Pinna, N.; Niederberger, M. *Angew. Chem., Int. Ed.* **2008**, *47*, 5292.
(70) Cooper, A. I. *Adv. Mater.* **2003**, *15*, 1049.
(71) Campbell, L. K.; Na, B. K.; Ko, E. I. *Chem. Mater.* **1992**, *4*, 1329.
(72) Suh, D. J.; Park, T.-J. *Chem. Mater.* **1996**, *8*, 509.
(73) Niederberger, M. *Acc. Chem. Res.* **2007**, *40*, 793.
(74) Leitner, W. *Acc. Chem. Res.* **2002**, *35*, 746.
(75) Brennecke, J. F.; Eckert, C. A. *AIChE J.* **1989**, *35*, 1409.
(76) Tadros, M. E.; Adkins, C. L. J.; Russick, E. M.; Youngman, M. P. *J. Supercrit. Fluids* **1996**, *9*, 172.
(77) Lim, K. T.; Hwang, H. S.; Lee, M. S.; Lee, G. D.; Hong, S.-S.; Johnston, K. P. *Chem. Commun.* **2002**, 1528.
(78) Lim, K. T.; Hwang, H. S.; Ryoo, W.; Johnston, K. P. *Langmuir* **2004**, *20*, 2466.
(79) Smith, P. G.; Ryoo, W.; Johnston, K. P. *J. Phys. Chem. B* **2005**, *109*, 20155.
(80) Loy, D. A.; Russick, E. M.; Yamanaka, S. A.; Baugher, B. M.; Shea, K. J. *Chem. Mater.* **1997**, *9*, 2264.
(81) Lucky, R. A.; Charpentier, P. A. *Adv. Mater.* **2008**, *20*, 1755.
(82) Sui, R.; Rizkalla, A. S.; Charpentier, P. A. *J. Phys. Chem. B* **2004**, *108*, 11886.
(83) Sui, R.; Rizkalla, A. S.; Charpentier, P. A. *Langmuir* **2005**, *21*, 6150.
(84) Sui, R.; Rizkalla, A. S.; Charpentier, P. A. *Langmuir* **2006**, *22*, 4390.
(85) Chowdhury, M. B. I.; Sui, R.; Lucky, R. A.; Charpentier, P. A. *Langmuir* **2010**, *26*, 2707.
(86) Sanchez, C.; Livage, J.; Henry, M.; Babonneau, F. *J. Non-Cryst. Solids* **1988**, *100*, 65.
(87) Sui, R.; Rizkalla, A. S.; Charpentier, P. A. *J. Phys. Chem. B* **2006**, *110*, 16212.
(88) Sui, R.; Thangadurai, V.; Berlinguette, C. P. *Chem. Mater.* **2008**, *20*, 7022.
(89) Moner-Girona, M.; Roig, A.; Molins, E. *J. Sol–Gel Sci. Technol.* **2003**, *26*, 645.
(90) Jespersen, H. T.; Standeker, S.; Novak, Z.; Schaumburg, K.; Madsen, J.; Knez, Z. *J. Supercrit. Fluids* **2008**, *46*, 178.
(91) Wang, J.; Xia, Y.; Wang, W.; Poliakoff, M.; Mokaya, R. *J. Mater. Chem.* **2006**, *16*, 1751.
(92) Reverchon, E.; Caputo, G.; Correra, S.; Cesti, P. *J. Supercrit. Fluids* **2003**, *26*, 253.
(93) Jensen, H.; Bremholm, M.; Nielsen, R. P.; Joensen, K. D.; Pedersen, J. S.; Birkedal, H.; Chen, Y.-S.; Almer, J.; Søgaard, E. G.; Iversen, S. B.; Iversen, B. B. *Angew. Chem., Int. Ed.* **2007**, *119*, 1131.
(94) Jensen, H.; Joensen, K. D.; Iversen, S. B.; Sogaard, E. G. *Ind. Eng. Chem. Res.* **2006**, *45*, 3348.
(95) Miao, Z.; Liu, Z.; Han, B.; Wang, Y.; Sun, Z.; Zhang, J. *J. Supercrit. Fluids* **2007**, *42*, 310.
(96) Stallings, W. E.; Lamb, H. H. *Langmuir* **2003**, *19*, 2989.

(97) Hong, S.-S.; Lee, M. S.; Lee, G.-D.; Lim, K. T.; Ha, B.-J. *Mater. Lett.* **2003**, *57*, 2975.
(98) Hong, S.-S.; Lee, M. S.; Ju, C.-S.; Lee, G.-D.; Park, S. S.; Lim, K.-T. *Catal. Today* **2004**, *93*−*95*, 871.
(99) Wu, C.-I.; Huang, J.-W.; Wen, Y.-L.; Wen, S.-B.; Shen, Y.-H.; Yeh, M.-Y. *Mater. Lett.* **2008**, *62*, 1923.
(100) Kellici, S.; Rehman, I.; Darr, J. *J. Mater. Chem.* **2006**, *16*, 159.
(101) Du, J.; Liu, Z.; Li, Z.; Han, B.; Huang, Y.; Gao, Y. *Microporous Mesoporous Mater.* **2005**, *83*, 19.
(102) Guo, G.; Whitesell, J. K.; Fox, M. A. *J. Phys. Chem. B* **2005**, *109*, 18781.
(103) Alonso, E.; Montequi, I.; Lucas, S.; Cocero, M. J. *J. Supercrit. Fluids* **2007**, *39*, 453.
(104) Lee, M.-H.; Lin, H.-Y.; Thomas, J. L. *J. Am. Ceram. Soc.* **2006**, *89*, 3624.
(105) Pessey, V.; Garriga, R.; Weill, F.; Chevalier, B.; Etourneau, J.; Cansell, F. *J. Mater. Chem.* **2002**, *12*, 958.
(106) Guizard, C.; Julbe, A.; Robbe, O.; Sarrade, S. *Catal. Today* **2005**, *104*, 120.
(107) Li, J.; Ma, H.; Cao, Y. *Adv. Mater. Res.* **2010**, *105*−*106*, 761.
(108) Sun, D.; Huang, Y.; Han, B.; Yang, G. *Langmuir* **2006**, *22*, 4793.
(109) Yoda, S.; Otake, K.; Takebayashi, Y.; Sugeta, T.; Sato, T. *J. Non-Cryst. Solids* **2001**, *285*, 8.
(110) Yoda, S.; Otake, K.; Takebayashi, Y.; Sugeta, T.; Sato, T. *J. Sol*−*Gel Sci. Technol.* **2000**, *19*, 719.
(111) Lucky, R. A.; Charpentier, P. A. *Sci. Adv. Mater.* **2009**, *1*, 167.
(112) Fu, L.; Liu, Y. Q.; Liu, Z. M.; Han, B. X.; Cao, L. C.; Wei, D. C.; Yu, G.; Zhu, D. B. *Adv. Mater.* **2006**, *18*, 181.
(113) Fu, L.; Liu, Z. M.; Liu, Y. Q.; Han, B. X.; Wang, J. Q.; Hu, P. A.; Cao, L. C.; Zhu, D. B. *Adv. Mater.* **2004**, *16*, 350.
(114) Sun, Z.; Yuan, H.; Liu, Z.; Han, B.; Zhang, X. *Adv. Mater.* **2005**, *17*, 2993.
(115) Sun, Z.; Zhang, X.; Na, N.; Liu, Z.; Han, B.; An, G. *J. Phys. Chem. B* **2006**, *110*, 13410.
(116) Pommier, C.; Chhor, K.; Bocquet, J. F.; Barj, M. *Mater. Res. Bull.* **1990**, *25*, 213.
(117) Chhor, K.; Bocquet, J. F.; Pommier, C. *Mater. Chem. Phys.* **1992**, *32*, 249.
(118) Vioux, A. *Chem. Mater.* **1997**, *9*, 2292.
(119) Mutin, P. H.; Vioux, A. *Chem. Mater.* **2009**, *21*, 582.
(120) Chhor, K.; Bocquet, J. F.; Pommier, C. *Mater. Chem. Phys.* **1995**, *40*, 63.
(121) Wang, X. M.; Xiao, P. *J. Mater. Res.* **2006**, *21*, 1189.
(122) Courtecuisse, V. G.; Bocquet, J. F.; Chhor, K.; Pommier, C. *J. Supercrit. Fluids* **1996**, *9*, 222.
(123) Znaidi, L.; Pommier, C. *Eur. J. Solid State Inorg. Chem.* **1998**, *35*, 405.
(124) Znaidi, L.; Chhor, K.; Pommier, C. *Mater. Res. Bull.* **1996**, *31*, 1527.
(125) Brasseur-Tilmant, J.; Pommier, C.; Chhor, K. *Mater. Chem. Phys.* **2000**, *64*, 156.
(126) Bocquet, J. F.; Chhor, K.; Pommier, C. *Surf. Coat. Technol.* **1994**, *70*, 73.
(127) Brasseur-Tilmant, J.; Chhor, K.; Jestin, P.; Pommier, C. *Mater. Res. Bull.* **1999**, *34*, 2013.
(128) Hald, P.; Becker, J.; Bremholm, M.; Pedersen, J. S.; Chevallier, J.; Iversen, S. B.; Iversen, B. B. *J. Solid State Chem.* **2006**, *179*, 2674.
(129) Reverón, H.; Aymonier, C.; Loppinet-Serani, A.; Elissalde, C.; Maglione, M.; Cansell, F. *Nanotechnology* **2005**, *16*, 1137.
(130) Bocquet, J. F.; Chhor, K.; Pommier, C. *Mater. Chem. Phys.* **1999**, *57*, 273.
(131) Elissalde, C.; Reverón, H.; Aymonier, C.; Michau, D.; Cansell, F.; Maglione, M. *Nanotechnology* **2005**, *16*, 797.
(132) Barj, M.; Bocquet, J. F.; Chhor, K.; Pommier, C. *J. Mater. Sci.* **1992**, *27*, 2187.
(133) Cabañas, A.; Li, J.; Blood, P.; Chudoba, T.; Lojkowski, W.; Poliakoff, M.; Lester, E. *J. Supercrit. Fluids* **2007**, *40*, 284.
(134) Oliver, S. A.; Hamdeh, H. H.; Ho, J. C. *Phys. Rev. B* **1999**, *60*, 3400.
(135) An, G.; Zhang, Y.; Liu, Z.; Miao, Z.; Han, B.; Miao, S.; Li, J. *Nanotechnology* **2008**, *19*, 1.
(136) An, G.; Ma, W.; Sun, Z.; Liu, Z.; Han, B.; Miao, S.; Miao, Z.; Ding, K. *Carbon* **2007**, *45*, 1795.
(137) Sun, Z.; Liu, Z.; Han, B.; Miao, S.; Du, J.; Miao, Z. *Carbon* **2006**, *44*, 888.
(138) Bavykin, D. V.; Friedrich, J. M.; Walsh, F. C. *Adv. Mater.* **2006**, *18*, 2807.
(139) Akiya, N.; Savage, P. E. *Chem. Rev.* **2002**, *102*, 2725.
(140) Danchevskaya, M. N.; Ivakin, Y. D.; Torbin, S. N.; Muravieva, G. P. *J. Supercrit. Fluids* **2007**, *42*, 419.
(141) Lester, E.; Blood, P.; Denyer, J.; Giddings, D.; Azzopardi, B.; Poliakoff, M. *J. Supercrit. Fluids* **2006**, *37*, 209.
(142) Galkin, A. A.; Kostyuk, B. G.; Kuznetsova, N. N.; Turakulova, A. O.; Lunin, V. V.; Polyakov, M. *Kinet. Catal.* **2001**, *42*, 154.
(143) Adschiri, T.; Kanazawa, K.; Arai, K. *J. Am. Ceram. Soc.* **1992**, *75*, 1019.
(144) Adschiri, T.; Kanazawa, K.; Arai, K. *J. Am. Ceram. Soc.* **1992**, *75*, 2615.
(145) Hakuta, Y.; Seino, K.; Ura, H.; Adschiri, T.; Takizawa, H.; Ara, K. *J. Mater. Chem.* **1999**, *9*, 2671.
(146) Li, G.; Smith, R. L.; Inomata, H.; Arai, K. *Mater. Lett.* **2002**, *53*, 175.
(147) Cabanas, A.; Darr, J. A.; Lester, E.; Poliakoff, M. *J. Mater. Chem.* **2001**, *11*, 561.
(148) Hakuta, Y.; Onai, S.; Terayama, H.; Adschiri, T.; Arai, K. *J. Mater. Sci. Lett.* **1998**, *17*, 1211.
(149) Cote, L. J.; Teja, A. S.; Wilkinson, A. P.; Zhang, Z. J. *J. Mater. Res.* **2002**, *17*, 2410.
(150) Ziegler, K. J.; Doty, R. C.; Johnston, K. P.; Korgel, B. A. *J. Am. Chem. Soc.* **2001**, *123*, 7797.
(151) Sue, K.; Suzuki, M.; Arai, K.; Ohashi, T.; Ura, H.; Matsui, K.; Hakuta, Y.; Hayashi, H.; Watanabe, M.; Hiaki, T. *Green Chem.* **2006**, *8*, 634.
(152) Xu, C.; Teja, A. S. *J. Supercrit. Fluids* **2006**, *39*, 135.
(153) Hao, Y.; Teja, A. S. *J. Mater. Res.* **2003**, *18*, 415.
(154) Cabanas, A.; Poliakoff, M. *J. Mater. Chem.* **2001**, *11*, 1408.
(155) Nilsen, M. H.; Nordhei, C.; Ramstad, A. L.; Nicholson, D. G.; Poliakoff, M.; Cabanas, A. *J. Phys. Chem. C* **2007**, *111*, 6252.
(156) Hayashi, H.; Torii, K. *J. Mater. Chem.* **2002**, *12*, 3671.
(157) Viswanathan, R.; Gupta, R. B. *J. Supercrit. Fluids* **2003**, *27*, 187.
(158) Ohara, S.; Mousavand, T.; Umetsu, M.; Takami, S.; Adschiri, T.; Kuroki, Y.; Takata, M. *Solid State Ionics* **2004**, *172*, 261.
(159) Sue, K.; Kimura, K.; Yamamoto, M.; Arai, K. *Mater. Lett.* **2004**, *58*, 3350.
(160) Hakuta, Y.; Adschiri, T.; Suzuki, T.; Chida, T.; Seino, K.; Arai, K. *J. Am. Ceram. Soc.* **1998**, *81*, 2461.
(161) Taboada, E.; Solanas, R.; Rodríguez, E.; Weissleder, R.; Roig, A. *Adv. Funct. Mater.* **2009**, *19*, 2319.
(162) Sorescu, M.; Diamandescu, L.; Tarabasanu-Mihaila, D. *J. Phys. Chem. Solids* **2004**, *65*, 1719.
(163) Cote, L. J.; Teja, A. S.; Wilkinson, A. P.; Zhang, Z. J. *Fluid Phase Equilib.* **2003**, *210*, 307.
(164) Galkin, A. A.; Kostyuk, B. G.; Lunin, V. V.; Poliakoff, M. *Angew. Chem., Int. Ed.* **2000**, *39*, 2738.
(165) Takesue, M.; Shimoyama, K.; Murakami, S.; Hakuta, Y.; Hayashi, H.; Smith, R. L., Jr. *J. Supercrit. Fluids* **2007**, *43*, 214.
(166) Lu, J.; Hakuta, Y.; Hayashi, H.; Ohashi, T.; Nagase, T.; Hoshi, Y.; Sato, K.; Nishioka, M.; Inoue, T.; Hamakawa, S. *J. Supercrit. Fluids* **2008**, *46*, 77.
(167) Hakuta, Y.; Haganuma, T.; Sue, K.; Adschiri, T.; Arai, K. *Mater. Res. Bull.* **2003**, *38*, 1257.
(168) Heller, W. *Polymer Colloidal II*; Plenum: New York, 1980.
(169) Vogelsberger, W.; Opfermann, J.; Wank, U.; Schulze, H.; Rudakoff, G. *J. Non-Cryst. Solids* **1992**, *145*, 20.
(170) Vogelsberger, W.; Seidel, A.; Fuchs, R. *J. Colloid Interface Sci.* **2000**, *230*, 268.

(171) Erriguible, A.; Marias, F.; Cansell, F.; Aymonier, C. *J. Supercrit. Fluids* **2009**, *48*, 79.
(172) Tanaka, N.; Kobayashi, H.; Nakanishi, K.; Minakuchi, H.; Ishizuka, N. *Anal. Chem.* **2001**, *73*, 420 A.
(173) Hara, T.; Kobayashi, H.; Ikegami, T.; Nakanishi, K.; Tanaka, N. *Anal. Chem.* **2006**, *78*, 7632.
(174) Tang, Q.; Xin, B.; Lee, M. L. *J. Chromatogr. A* **1999**, *837*, 35.
(175) Sui, R.; Liu, S.; Lajoie, G. A.; Charpentier, P. A. *J. Sep. Sci.* **2010**, *33*, 1604.
(176) Sharp, K. G. *J. Sol−Gel Sci. Technol.* **1994**, *2*, 35.
(177) Sui, R.; Rizkalla, A. S.; Charpentier, P. A. *Cryst. Growth Des.* **2008**, *8*, 3024.
(178) Charpentier, P. A.; Li, X.; Sui, R. *Langmuir* **2009**, *25*, 3748.
(179) Arai, H.; Machida, M. *Appl. Catal., A* **1996**, *138*, 161.
(180) Al-Yassir, N.; Le Van Mao, R. *Appl. Catal., A* **2007**, *317*, 275.
(181) Vollet, D. R.; de Sousa, W. A. T.; Donatti, D. A.; Ibañez Ruiz, A. *J. Non-Cryst. Solids* **2007**, *353*, 143.
(182) Bisson, A.; Rigacci, A.; Lecomte, D.; Achard, P. *J. Non-Cryst. Solids* **2004**, *350*, 379.
(183) Pajonk, G. M.; Elaloui, E.; Achard, P.; Chevalier, B.; Chevalier, J.-L.; Durant, M. *J. Non-Cryst. Solids* **1995**, *186*, 1.
(184) Teichner, S. J.; Nicolaon, G. A.; Vicarini, M. A.; Gardes, G. E. E. *Adv. Colloid Interface Sci.* **1976**, *5*, 245.
(185) Calvino, J. J.; Cauqui, M. A.; Cifredo, G.; Esquivias, L.; Pérez, J. A.; Solar, M. R.; Rodríguez-Izquierdo, J. M. *J. Mater. Sci.* **1993**, *28*, 2191.
(186) Grandi, S.; Costa, L. *J. Non-Cryst. Solids* **1998**, *225*, 141.
(187) Suh, D. J.; Park, T.-J.; Han, H.-Y.; Lim, J.-C. *Chem. Mater.* **2002**, *14*, 1452.
(188) Zhang, C.; Zhang, J.; Zhang, X.; Feng, X.; Chen, J.; Han, B.; Yang, G. *J. Supercrit. Fluids* **2007**, *42*, 142.
(189) Zhang, J.; Liu, Z.; Han, B.; Li, Z.; Yang, G.; Li, J.; Chen, J. *J. Supercrit. Fluids* **2006**, *36*, 194.
(190) Wang, J.; Xia, Y.; Wang, W.; Mokaya, R.; Poliakoff, M. *Chem. Commun.* **2005**, 210.
(191) Zhao, Y.; Zhang, J.; Li, W.; Zhang, C.; Han, B. *Chem. Commun.* **2009**, 2365.
(192) Volmer, M.; Esterman, J. *Z. Phys* **1921**, *7*, 13.
(193) Iijima, S. *Nature* **1991**, *354*, 56.
(194) Xia, Y.; Yang, P.; Sun, Y.; Wu, Y.; Mayers, B.; Gates, B.; Yin, Y.; Kim, F.; Yan, H. *Adv. Mater.* **2003**, *15*, 353.
(195) Kuchibhatla, S. V. N. T.; Karakoti, A. S.; Bera, D.; Seal, S. *Prog. Mater. Sci.* **2007**, *52*, 699.
(196) Wang, Y.; Liu, Z.; Han, B.; Sun, Z.; Du, J.; Zhang, J.; Jiang, T.; Wu, W.; Miao, Z. *Chem. Commun.* **2005**, 2948.
(197) Wakayama, H.; Itahara, H.; Tatsuda, N.; Inagaki, S.; Fukushima, Y. *Chem. Mater.* **2001**, *13*, 2392.
(198) Sui, R.; Charpentier, P. A.; Rizkalla, A. S.; Jennings, M. C. *Acta Crystallogr., Sect. E* **2006**, *62*, No. m373.
(199) Lucky, R. A.; Sui, R.; Charpentier, P. A.; Jennings, M. C. *Acta Crystallogr., Sect. E* **2007**, *63*, No. m2429.
(200) Lucky, R. A.; Charpentier, P. A. *Nanotechnology* **2009**, *20*, 1.
(201) Moner-Girona, M.; Roig, A.; Benito, M.; Molins, E. *J. Mater. Chem.* **2003**, *13*, 2066.
(202) Ghosh, K.; Vyas, S. M.; Lehmler, H. J.; Rankin, S. E.; Knutson, B. L. *J. Phys. Chem. B* **2007**, *111*, 363.
(203) Su, L.; Pei, S.; Li, L.; Li, H.; Zhang, Y.; Yu, W.; Zhou, C. *Int. J. Hydrogen Energy* **2009**, *34*, 6892.
(204) Zou, H.; Wu, S.; Shen, J. *Chem. Rev.* **2008**, *108*, 3893.
(205) Yue, B.; Yang, J.; Huang, C.-Y.; Dave, R.; Pfeffer, R. *Macromol. Rapid Commun.* **2005**, *26*, 1406.
(206) Sun, D.; Zhang, R.; Liu, Z.; Huang, Y.; Wang, Y.; He, J.; Han, B.; Yang, G. *Macromolecules* **2005**, *38*, 5617.
(207) Tatsuda, N.; Itahara, H.; Setoyama, N.; Fukushima, Y. *Carbon* **2005**, *43*, 2358.
(208) Tatsuda, N.; Itahara, H.; Setoyama, N.; Fukushima, Y. *J. Mater. Chem.* **2004**, *14*, 3440.
(209) Yoda, S.; Sakurai, Y.; Endo, A.; Miyata, T.; Otake, K.; Yanagishita, H.; Tsuchiya, T. *Chem. Commun.* **2002**, 1526.
(210) Miao, S.; Liu, Z.; Han, B.; Zhang, J.; Yu, X.; Du, J.; Sun, Z. *J. Mater. Chem.* **2006**, *16*, 579.
(211) Yoda, S.; Sakurai, Y.; Endo, A.; Miyata, T.; Yanagishita, H.; Otake, K.; Tsuchiya, T. *J. Mater. Chem.* **2004**, *14*, 2763.
(212) Fu, L.; Liu, Z.; Liu, Y.; Han, B.; Hu, P.; Cao, L.; Zhu, D. *Adv. Mater.* **2005**, *17*, 217.
(213) Liu, Z.; Han, B. *Adv. Mater.* **2009**, *21*, 825.
(214) Sun, D.; Liu, Z.; He, J.; Han, B.; Zhang, J.; Huang, Y. *Microporous Mesoporous Mater.* **2005**, *80*, 165.
(215) Charpentier, P. A.; Xu, W. Z.; Li, X. *Green Chem.* **2007**, *9*, 768.
(216) Tatsuda, N.; Fukushima, Y.; Wakayama, H. *Chem. Mater.* **2004**, *16*, 1799.
(217) Wakayama, H.; Goto, Y.; Fukushima, Y. *Phys. Chem. Chem. Phys.* **2003**, *5*, 3784.
(218) Wakayama, H.; Fukushima, Y. *Chem. Mater.* **2000**, *12*, 756.
(219) Wakayama, H.; Fukushima, Y. *Ind. Eng. Chem. Res.* **2000**, *39*, 4641.
(220) Wakayama, H.; Fukushima, Y. *Ind. Eng. Chem. Res.* **2006**, *45*, 3328.
(221) Wakayama, H.; Inagaki, S.; Fukushima, Y. *J. Am. Ceram. Soc.* **2002**, *85*, 161.
(222) Fukushima, Y.; Wakayama, H. *J. Phys. Chem. B* **1999**, *103*, 3062.
(223) Crowley, T. A.; Ziegler, K. J.; Lyons, D. M.; Erts, D.; Olin, H.; Morris, M. A.; Holmes, J. D. *Chem. Mater.* **2003**, *15*, 3518.
(224) Xu, Q.; Ding, K.; He, L.; Li, J.; Guo, Y.; Fan, H. *Mater. Sci. Eng., B* **2005**, *121*, 266.
(225) Xu, Q.; Fan, H.; Guo, Y.; Cao, Y. *Mater. Sci. Eng., A* **2006**, *435−436*, 158.
(226) Miao, Z.; Ding, K.; Wu, T.; Liu, Z.; Han, B.; An, G.; Miao, S.; Yang, G. *Microporous Mesoporous Mater.* **2008**, *111*, 104.
(227) Li, J.; Shi, X.; Wang, L.; Liu, F. *J. Colloid Interface Sci.* **2007**, *315*, 230.
(228) Fan, H.; Xu, Q.; Guo, Y.; Cao, Y. *Ind. Eng. Chem. Res.* **2006**, *45*, 5009.
(229) Cabanas, A.; Enciso, E.; Carbajo, M. C.; Torralvo, M. J.; Pando, C.; Renuncio, J. A. R. *Chem. Commun.* **2005**, 2618.
(230) Cabanas, A.; Enciso, E.; Carbajo, M. C.; Torralvo, M. J.; Pando, C.; Renuncio, J. A. R. *Chem. Mater.* **2005**, *17*, 6137.
(231) Cabanas, A.; Enciso, E.; Carmen Carbajo, M.; Torralvo, M. J.; Pando, C.; Renuncio, J. A. R. *Microporous Mesoporous Mater.* **2007**, *99*, 23.
(232) Tenorio, M. J.; Torralvo, M. J.; Enciso, E.; Pando, C.; Renuncio, J. A. R.; Cabañas, A. *J. Supercrit. Fluids* **2009**, *49*, 369.
(233) Chen, Z.; Li, S.; Xue, F.; Sun, G.; Luo, C.; Chen, J.; Xu, Q. *Colloids Surf., A* **2010**, *355*, 45.
(234) Van Eldik, R.; Asano, T.; Le Noble, W. J. *Chem. Rev.* **1989**, *89*, 549.
(235) Zhang, Z.; Wu, W.; Han, B.; Jiang, T.; Wang, B.; Liu, Z. *J. Phys. Chem. B* **2005**, *109*, 16176.
(236) Hou, Z.; Han, B.; Zhang, X.; Zhang, H.; Liu, Z. *J. Phys. Chem. B* **2001**, *105*, 4510.
(237) Ghosh, R.; Nethaji, M.; Samuelson, A. G. *Chem. Commun.* **2003**, 2556.
(238) Gupta, R. B.; Shim, J.-J. *Solubility in Supercritical Carbon Dioxide*; CRC Press: Boca Raton, FL, U.S.A., 2007.
(239) Lu, B.; Zhang, D.; Sheng, W. *Pure Appl. Chem.* **1990**, *62*, 2277.
(240) Sui, R.; Lo, J. M. H.; Charpentier, P. A. *J. Phys. Chem. C* **2009**, *113*, 21022.
(241) Kazarian, S. G.; Vincent, M. F.; Bright, F. V.; Liotta, C. L.; Eckert, C. A. *J. Am. Chem. Soc.* **1996**, *118*, 1729.
(242) Bamberger, A.; Sieder, G.; Maurer, G. *J. Supercrit. Fluids* **2000**, *17*, 97.
(243) Bamberger, A.; Sieder, G.; Maurer, G. *J. Supercrit. Fluids* **2004**, *32*, 15.
(244) Panagiotopoulos, A. Z.; Willson, R. C.; Reid, R. C. *J. Chem. Eng. Data* **1988**, *33*, 321.
(245) M'Hamdi, R.; Bocquet, J. F.; Chhor, K.; Pommier, C. *J. Supercrit. Fluids* **1992**, *5*, 55.

(246) Matson, D. W.; Smith, R. D. *J. Am. Ceram. Soc.* **1989**, *72*, 871.
(247) Morey, G. W. *Econ. Geol.* **1957**, *52*, 225.
(248) Kennedy, G. C. *Econ. Geol.* **1950**, *45*, 629.
(249) Prausnitz, J. M.; Lichtenthaler, R. N.; Azevedo, E. G. d. *Molecular Thermodynamics of Fluid-Phase Equilibria*, 3rd ed.; Prentice Hall PTR: Upper Saddle River, NJ, U.S.A., 1999.
(250) Johnston, K. P.; Peck, D. G.; Kim, S. *Ind. Eng. Chem. Res.* **1989**, *28*, 1115.
(251) Gmehling, J. *Fluid Phase Equilib.* **1998**, *144*, 37.
(252) Fried, J. R. *Polymer Science and Technology*, 2nd ed.; Prentice Hall Professional Technical Reference: Upper Saddle River, NJ, U.S.A., 2003.
(253) Fedors, R. F. *Polym. Eng. Sci.* **1974**, *14*, 147.
(254) Fedors, R. F. *Polym. Eng. Sci.* **1974**, *14*, 472.
(255) Lucky, R. A.; Sui, R.; Lo, J. M. H.; Charpentier, P. A. *Cryst. Growth Des.* **2010**, *10*, 1598.
(256) Peters, C. J.; Gauter, K. *Chem. Rev.* **1999**, *99*, 419.
(257) Cansell, F.; Aymonier, C.; Loppinet-Serani, A. *Curr. Opin. Solid State Mater. Sci.* **2003**, *7*, 331.
(258) Desmoulins-Krawiec, S.; Aymonier, C.; Loppinet-Serani, A.; Weill, F.; Gorsse, S.; Etourneau, J.; Cansell, F. *J. Mater. Chem.* **2004**, *14*, 228.
(259) Matijevic, E.; Sapieszko, R. S. In *Fine Particles: Synthesis, Characterization, and Mechanisms of Growth*; Sugimoto, T., Ed.; CRC Press: Boca Raton, FL, U.S.A., 2000.
(260) Gourinchas Courtecuisse, V.; Chhor, K.; Bocquet, J.-F.; Pommier, C. *Ind. Eng. Chem. Res.* **1996**, *35*, 2539.
(261) Dickson, J. L.; Gupta, G.; Horozov, T. S.; Binks, B. P.; Johnston, K. P. *Langmuir* **2006**, *22*, 2161.
(262) Bremholm, M.; Jensen, H.; Iversen, S. B.; Iversen, B. B. *J. Supercrit. Fluids* **2008**, *44*, 385.
(263) Romang, A. H.; Watkins, J. J. *Chem. Rev.* **2010**, *110*, 459.
(264) Sedach, P. A.; Gordon, T. J.; Sayed, S. Y.; Furstenhaupt, T.; Sui, R.; Baumgartner, T.; Berlinguette, C. P. *J. Mater. Chem.* **2010**, *20*, 5063.
(265) Hochbaum, A. I.; Yang, P. *Chem. Rev.* **2010**, *110*, 527.
(266) Hansen, B. N.; Hybertson, B. M.; Barkley, R. M.; Sievers, R. E. *Chem. Mater.* **1992**, *4*, 749.
(267) Llusar, M.; Sanchez, C. *Chem. Mater.* **2008**, *20*, 782.
(268) Kawakami, K.; Urakawa, T.; Oda, Y.; Iwai, Y. *J. Chem. Technol. Biotechnol.* **2009**, *84*, 1412.
(269) George, M. W.; Poliakoff, M.; Turner, J. J. *Analyst* **1994**, *119*, 551.
(270) Sun, X.-Z.; Grills, D. C.; Nikiforov, S. M.; Poliakoff, M.; George, M. W. *J. Am. Chem. Soc.* **1997**, *119*, 7521.
(271) Dardin, A.; DeSimone, J. M.; Samulski, E. T. *J. Phys. Chem. B* **1998**, *102*, 1775.
(272) Horvath, I. T.; Millar, J. M. *Chem. Rev.* **1991**, *91*, 1339.
(273) Amita, F.; Oka, H.; Mukaide, M.; Urasaki, Y.; Takegoshi, K.; Terao, T.; Kajimoto, O. *Rev. Sci. Instrum.* **2004**, *75*, 467.
(274) Masten, D. A.; Foy, B. R.; Harradine, D. M.; Dyer, R. B. *J. Phys. Chem.* **1993**, *97*, 8557.